crystals

MDPI

Article

Supramolecular Assemblies of 3/4-Chlorobenzoic Acid and Amino-Chloropyridine Derivatives: Synthesis, X-ray Diffraction, DFT Calculations, and Biological Screening

Tufail Ahmad [1], Naveen Kosar [2], Muhammad Said [1], Maqsood Ahmed [3], Tariq Mahmood [4,5] and Ezzat Khan [1,4,*]

[1] Department of Chemistry, University of Malakand, Chakdara 18800, Pakistan; tufailahmad043@gmail.com (T.A.)
[2] Department of Chemistry, University of Management and Technology (UMT), Johar Town, Lahore 54770, Pakistan
[3] Materials Chemistry Laboratory, Institute of Chemistry, The Islamia University of Bahawalpur, Baghdad ul Jaded Campus, Bahawalpur 63100, Pakistan
[4] Department of Chemistry, College of Science, University of Bahrain, Main Campus, Zallaq 32038, Bahrain
[5] Department of Chemistry, COMSATS University Islamabad, Abbottabad Campus, Abbottabad 22060, Pakistan
* Correspondence: ekhan@uom.edu.pk

Abstract: Organic acids (3-chlorobenzoic acid and 4-chlorobenzoic acid) were treated with 4-amino-2-chloropyridine and 2-amino-4-chloropyridine as coformers for cocrystallization. Acid/base pairs afforded a cocrystal (3-chlorobenzoic acid and 4-amino-2-chloropyridine, compound **1**) and molecular salts (2-amino-4-chloropyridinium 3-chlorobenzoate, **2**; 2-amino-4-chloropyridinium 4-chlorobenzoate, **3**). The products were characterized with the help of FT-IR, UV/visible spectroscopy, PXRD, and SC-XRD. The position of the Cl-substituent on the phenyl ring was explored with respect to proton transfer between acid/base pairs, and its role in supramolecular chemistry is discussed in detail. The existence of supramolecular assemblies was further reproduced using DFT calculations. Further, frontier molecular orbital (FMO), molecular electrostatic potential (MEP), and noncovalent interaction index (NCI) analyses were performed to gain insight into the electronic properties and nature of noncovalent interactions. The prepared compounds were examined for their biological activities against selected Gram-positive and Gram-negative bacterial strains and were also tested as antioxidant agents (DPPH free radical scavenging). Structural parameters determined experimentally and theoretically are within the expected range, and the biological activities of the resultant compounds are moderate.

Keywords: molecular salts; aminopyridinium benzoate; Cl-Cl interactions; supramolecular chemistry; DFT calculations; antioxidant and antibacterial studies

Citation: Ahmad, T.; Kosar, N.; Said, M.; Ahmed, M.; Mahmood, T.; Khan, E. Supramolecular Assemblies of 3/4-Chlorobenzoic Acid and Amino-Chloropyridine Derivatives: Synthesis, X-ray Diffraction, DFT Calculations, and Biological Screening. *Crystals* **2023**, *13*, 1663. https://doi.org/10.3390/cryst13121663

Academic Editors: Michał K. Cyrański and Jesús Sanmartín-Matalobos

Received: 16 September 2023
Revised: 28 November 2023
Accepted: 30 November 2023
Published: 5 December 2023

1. Introduction

Molecular salts and cocrystals are competitive products obtained via reactions between weak organic acids and bases. The resultant materials are collectively considered multi-component crystals which can be distinguished from each other on the basis of the transfer of at least one proton [1,2]. The formation of salts and/or cocrystals is carried out for the enhancement of physicochemical properties like solubility, dissolution, bioavailability, and stability and for pharmaceutical purposes [3]. The ionization constant gives important information about the degree of proton transfer or the ability of salt formation to resist the disproportionation of the involved synthons [4]. The formulation of new supramolecular assemblies without breaking existing covalent bonds is the beauty of crystal engineering in which intermolecular interactions are responsible for holding synthons together [5,6]. Various non-covalent interactions like hydrogen bonding [7–10], halogen bonds [11–15], van der Waals interactions, and π–π stacking [16–18] play an important role in this regard.

Similar to hydrogen bonding, halogen bonding is also considered significant in the packing of crystal structures [19–21]. Resnati and Merangolo et al. briefly explained the importance of halogen bonding in crystal packing and nature in the multicomponent structure of an iodoperflurocarbon with aliphatic amines [22,23]. Both hydrogen and halogen bonds coexist within the same crystal structure, which tunes the properties in an engineered way in the cocrystals/salts of thiophene carboxylic acids and nitrogenous bases [24]. Halogen bonds play a role in designing functional materials in the fields of optics, photonics, biomimetics, photo-switchable and functional surface supramolecules [25].

The non-covalent interactions between halogen atoms and donor atoms like N, O, and S are considered efficient for holding synthons together [26,27]. From both theoretical and experimental studies, it can be determined that electron clouds are anisotropically distributed along with covalently held halogen atoms [28,29]. This causes a minute localized positive potential region known as the σ-hole [30]. Thus, a nucleophilic atom can interact with the σ-hole, and a halogen bond is formed [31,32]. Sometimes, halogen–halogen interactions appear when both electrophilic and nucleophilic interactions coexist on a halogen atom; these are also termed σ-hole–σ-hole interactions [33,34]. Halogen roles are vital in pharmaceutical products wherein the concept of halogen-based supramolecular assemblies is worth exploring. In this regard, the first example of a pharmaceutical cocrystal based on halogen bonds was reported by Baldrighi et al. in 2013 [35]. The halogen atoms in the drug molecules may result in increased permeability which, in turn, leads to an increase in oral bioavailability [36].

Pyridine is a well-known heterocycle which plays a role as a central ring in many organic compounds [37]. Its effects against various ailments as medicine have been shown, and is a good Lewis base, causing its derivatives to have attractive ligands to accept protons and bind to metal centers [38–41]. Several halogenated derivatives of pyridine and organic acids have been well characterized, and their properties have been explored [42]. The multicomponent structure as a product can be efficiently predicted from Rule of 3. According to this rule, molecular salt formation is dominant over cocrystals if $\Delta pK_a > 3$ (ΔpK_a is the difference between pK_a (base) and pK_a (acid)), while cocrystals are formed if $\Delta pK_a < 3$ [43]. If this difference in pK_a is closer to or equal to 3, either product can be obtained [44,45]. Carboxylic functionality shows efficiency in establishing hydrogen bonds with a suitable coformer (base) like pyridine and amine derivatives [46].

Here, we report the molecular salts of 3-chlorobenzoic acid/4-amino-2-chloropyridine, 3-chlorobenzoic acid/2-amino-4-chloropyridine, and 4-chlorobenzoic acid/2-amino-4-chloropyridine (Scheme 1). The incorporation of a chloro-group led to weak Van der Waals interactions and interesting supramolecular chemistry, but the final products as molecular salts/cocrystals were obtained as expected for the difference in p*K*a of the starting material. The supramolecular chemistry of isolated synthons was discussed, and their biological applications were explored.

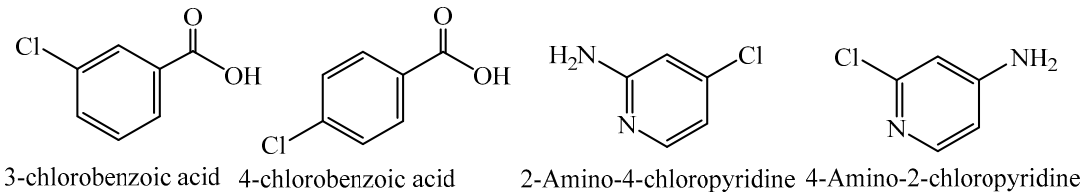

Scheme 1. Organic acids and bases used in this study.

2. Results and Discussion

In the current work, heterosynthons were selected according to the availability of donor–accepter sites for noncovalent interactions. Chloro functionality at various positions of the principal aromatic rings of both acids and bases in molecules was considered in which the position of the halogen affects its role in secondary interactions. In a continuation of previous work on non-covalent interactions and multicomponent structure design [39,47,48], new products are hereby presented from the reaction of benzoic acid derivatives and pyridine deriva-

tives. The pK_a values of 3-chlorobenzoic acid, 4-chlorobenzoic acid, 4-Amino-2-cholorpyridine, and 2-Amino-4-cholorpyridine are 3.85, 3.98, 4.73 and 5.72, respectively [49]. In case of compounds **1** (3-chlorobenzoic acid/4-amino-2-chloropyridine) and **2** (2-amino-4-chloropyridinium 3-chlorobenzoate) and **3** (2-amino-4-chloropyridinium 4-chlorobenzoate), the difference in the value of pK_a is less than 3 (ΔpK_a = 0.88, 1.87, and 1.74, respectively) so, according to Rule 3, cocrystal formation dominates. The role of the structure of coformers is more active in comparison with the "Rule of 3," particularly the presence of the pyridine ring, which is more basic and has a greater affinity to accept H^+ [47].

2.1. Physical Phase Diagram of the Starting Materials of Compounds **1**, **2**, *and* **3**

The physical mixture of the starting materials of compound **1** (3-chlorobenzoic acid and 4-Amino-2-chloropyridine) were prepared in different molar ratios, 1:9, 2:8, 3:7, 4:6, 5:5, 6:4, 7:3, 8:2, and 9:1, in a solid state. The nine different physical mixtures of the components of 3-chlorobenzoic acid (in the case of compound **2**) and 4-chlorobenzoic acid (in the case of compound **3**) with 2-amino-4-chloropyridine were prepared in the same way as discussed above. A zigzag pattern (W-type) in the melting points of the physical mixtures is an indication of physical interactions. It is a well-established fact that cocrystals and the physical mixture of their coformers have different melting points [50,51]. In a similar way, binary phase and ternary phase diagrams are easy methods of determining solubility as a function of physical interactions. In this regard, a phase diagram of a physical mixture of the coformers of cinnamic acid and nicotinamide is reported as a case study [52]. The melting point of mixture does not follow a regular pattern, as shown in Figure 1, which confirms that both conformers interact with each other via physical interactions like hydrogen bonding, halogen bonding, or other non-covalent interactions.

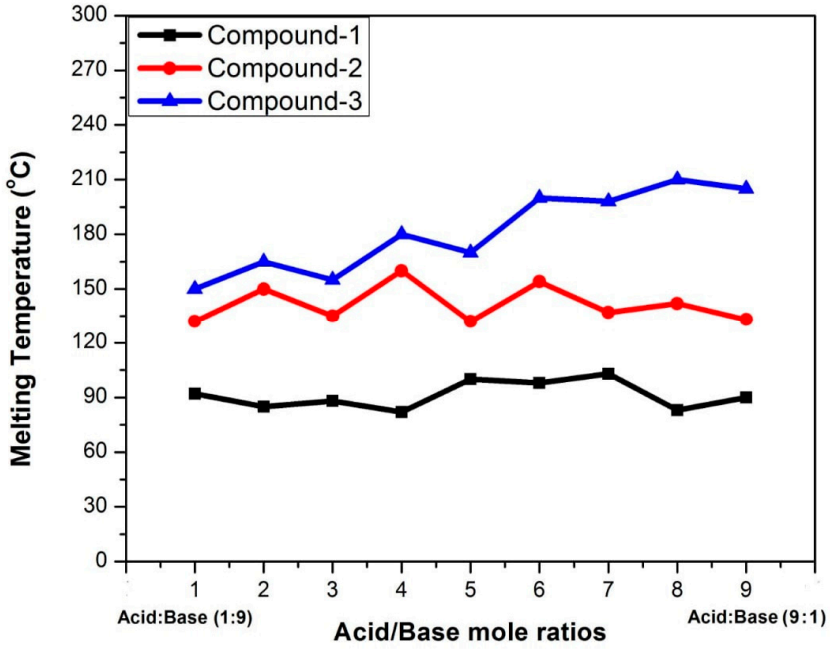

Figure 1. Physical phase diagram revealing the melting temperatures of mixtures of the starting precursors used in the synthesis of compounds **1**–**3**. It indicates physical interactions between the components in various molar ratios. Different colour are used to distinguish compounds from each other as shown at the top of the figure.

2.2. FT-IR Studies of Compounds **1**, **2** *and* **3**

The FT-IR spectra of both starting materials (synthons) and their resultant multicomponent structures were recorded and correlated (shown in Figures S1–S3). In the spectrum of compound **1**, a weak broad absorption at 3350 cm^{-1} can be assigned to an OH group. Extensive hydrogen bonding in the cocrystal is evident from a shift toward

a lower wavenumber and the broadness of the peak when compared with the starting acid. The same phenomenon was observed with the N-H bond of aminopyridine, for which a shift occurs from 3300 cm^{-1} to a weak and broad peak at 3200–3300 cm^{-1}. Other peaks of the starting materials and resultant products appear with slight shifts because of the involvements of some of the groups in secondary interactions. In the spectrum of compound **2**, the O-H bond ≈ 3560 cm^{-1} disappears, indicating the transfer of a proton from the acid molecule, which clearly supports the formation of a molecular salt. Also, the N-H bonds of aminopyridine are involved in noncovalent interactions with coformers. The aromatic C-H bonds appear in their expected region.

2.3. Powder and Single X-Ray Diffraction Studies of Compounds **1**–**3**

The powder X-ray diffraction patterns of compounds **1** (cocrystal), **2**, and **3** (molecular salts) are given in Figures S5–S7. From the regularity of the peaks in the pattern, the crystalline nature of the compounds is confirmed. The same pattern of peak intensities can also be achieved from single-crystal X-ray diffraction using a simulated powder pattern. These spectra reveal that the bulk of the compounds obtained in this study are reasonably pure, with negligible side reactions and side products. Further confirmation of the structural characterization of the compounds was carried out for single crystals of all the compounds.

2.4. Single X-Ray Structural Description of Cocrystal of 3-Chlorobenzoic Acid:4-Amino-2-Chloropyridine, Compound **1**

The molecular structure of compound **1** is shown in Figure 2; it crystallizes in the $P2_1$ space group. It is evident from the single-crystal analysis of compound **1** that secondary interactions give extra stability to the compound in a solid state. Interactions between OH---N (where the OH of the acid and the N of the pyridine ring) appear with a separation distance between N(2) and H(2) equal to 1.633 Å. This is the only H-bonding interaction with the help of which an acid/base pair is held together. H^+ transfer in an acid/base pair does not take place under the provided conditions. The pyridine and phenyl ring of the acid are twisted with respect to each other at approximately 45°. Further, each NH_2 and C=O group is involved in intermolecular H-bonding and stabilizing the supramolecular structure of the co-crystal. The distance between N(1)H and O(1) is 2.019 Å. As a result of H-bonding, the chair structure extends in a 1D fashion, as shown in Figure 3. The chloro functionalities of both the heterosynthons' acids and bases interact with each other through van der Waals forces with a separation distance of Cl(1)---Cl(01) 3.497 Å, and at the same time, Cl(01), which belongs to benzoic acid moiety, is associated with an ammine group of the base, and Cl(01)---HN is equal to 2.683 Å. In contrast to H-bonding (discussed above), Cl---Cl interactions stabilize the 2D extension of the supramolecular structure. There are some other interactions which, collectively with Cl---Cl and H-bonding, afford a 3D structure in a solid state. The main role played by the aromatic ring of the acidic moiety is obvious in stabilizing the 3D supramolecular structure of the molecule. The C=O---HN bonds are the main forces which hold molecules together in a solid state (Figure 2), while halogen interactions can be observed among all nearby halogen atoms (Cl atoms), as shown in Figure 3. Data pertaining to crystal structure refinements and solutions are summarized in Table 1. In the crystal structure of the compound, each acid molecule is attached to four pyridine derivatives, one of which is attached with the help of a halogen–halogen interaction. In the case of 4-Amino-2-chloropyridine, four different acid molecules are attached, one of which is because of halogen bonding, while the remaining are attached with hydrogen bonds. The C(1) of benzoic acid is linked to the C(6) of another acidic moiety through π–π interactions (C(1)---C(6); 3.397 Å), extending the straight chain of acidic groups. Two parallel chains of acids are associated with each other via C(5)H---C(2) interactions which are separated by 3.781 Å, while the H(5)---C(2) distance is 2.855 Å (Figure 4). Such interactions are not present within base molecules.

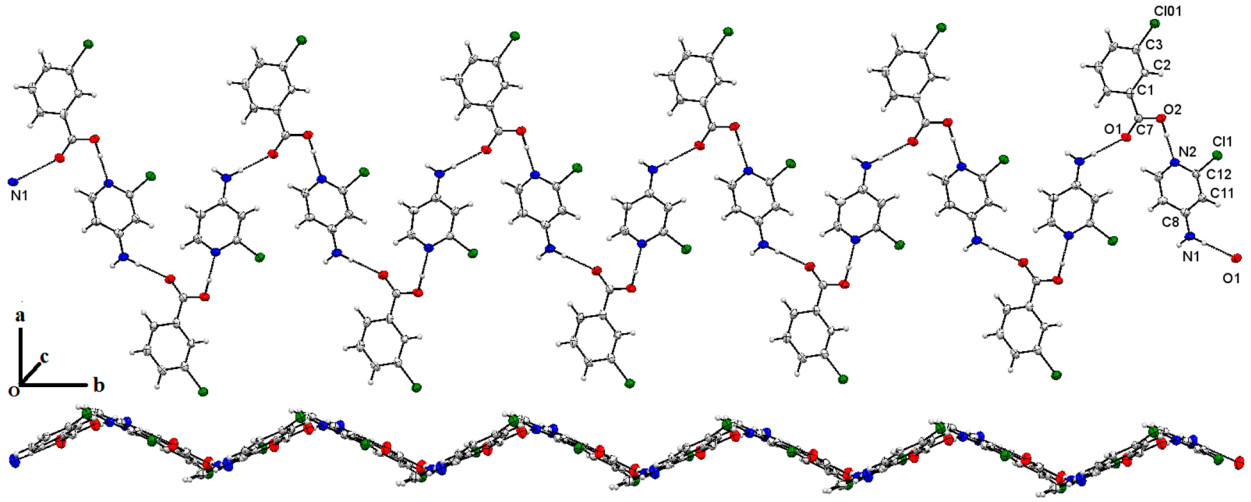

Figure 2. One-dimensional Molecular extension of a 1:1 cocrystal of 3-chlorobenzoic acid:4-Amino-2-chloropyridine. Acid-base are made as a result of NH-O interactions and the respective pairs are linked through NH_2---O=C bonds (Uniform color scheme is used for all molecules as; red = oxygen, blue = nitrogen and green = chlorine atoms).

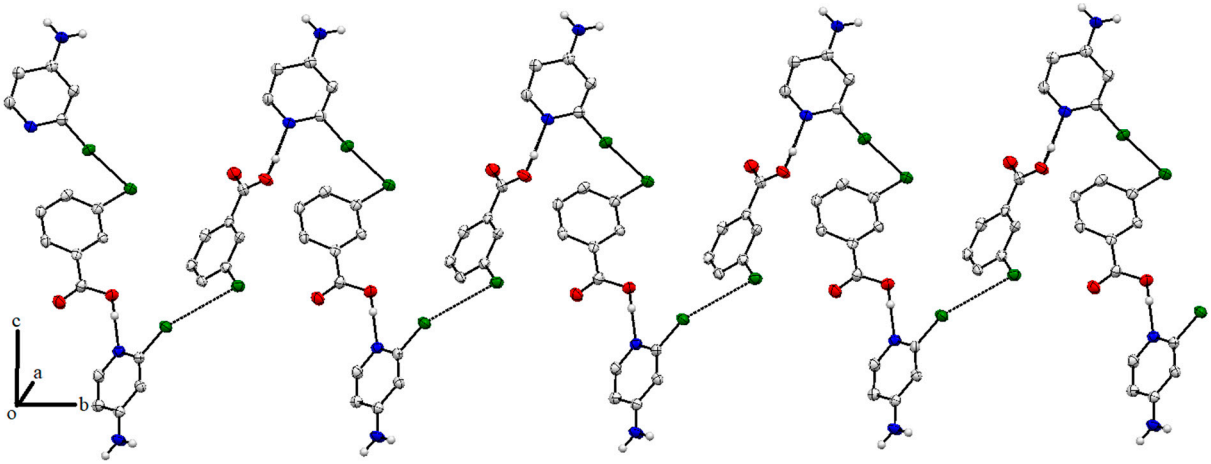

Figure 3. Halogen bonding among heterosynthons of compound **1**.

Table 1. Experimental details of compounds **1**–**3**.

	Compound 1	**Compound 2**	**Compound 3**
Chemical formula	$C_7H_5ClO_2{\cdot}C_5H_5ClN_2$	$C_7H_4ClO_2{\cdot}C_5H_6ClN_2$	$0.5(C_7H_4ClO_2){\cdot}0.5(C_5H_4ClN_2)$
M_r	285.13	285.13	141.56
Crystal system, space group	Monoclinic, $P2_1$	Monoclinic, $P2_1$	Monoclinic, P_c
Temperature (K)	150	150	150
a, b, c (Å)	3.7979 (4), 11.4738 (11), 14.0722 (15)	8.0024 (16), 6.8306 (12), 11.1631 (18)	10.0269 (10), 5.1405 (6), 12.1494 (15)
β (°)	92.088 (4)	93.656 (5)	90.678 (4)
V (Å^3)	612.81 (11)	608.95 (19)	626.18 (12)
Z	2	2	4
Radiation type	Mo $K\alpha$	Mo $K\alpha$	Mo $K\alpha$

Table 1. *Cont.*

	Compound 1	Compound 2	Compound 3
μ (mm^{-1})	0.52	0.53	0.51
Crystal size (mm)	0.17 × 0.16 × 0.11	0.24 × 0.16 × 0.12	0.27 × 0.33 × 0.37
Data collection			
Diffractometer	Bruker D8 VENTURE PHOTON II with Oxford COBRA Cryosystem		
Absorption correction	Multi-scan	Multi-scan	Multi-scan
No. of measured, independent, and observed [I ≥ 2u(I)] reflections	2460, 2460, 2048	12465, 2473, 1653	9501, 2433, 1516
R_{int}	0.022	0.126	0.059
$(\sin\theta/\lambda)_{max}$ ($Å^{-1}$)	0.624	0.624	0.626
$R[F^2 > 2\sigma(F^2)]$, $wR(F^2)$, S	0.046, 0.110, 1.08	0.051, 0.112, 1.08	0.125, 0.445, 1.71
No. of reflections	2460	2473	2433
No. of parameters	167	173	163
No. of restraints	1	1	2
H-atom treatment	H-atom parameters constrained		
$\Delta\rho_{max}$, $\Delta_{\rho min}$ (e $Å^{-3}$)	0.58, −0.33	0.50, −0.56	0.85, −0.91
Absolute structure parameter	−0.04 (10)	0.02 (12)	0.56 (6)

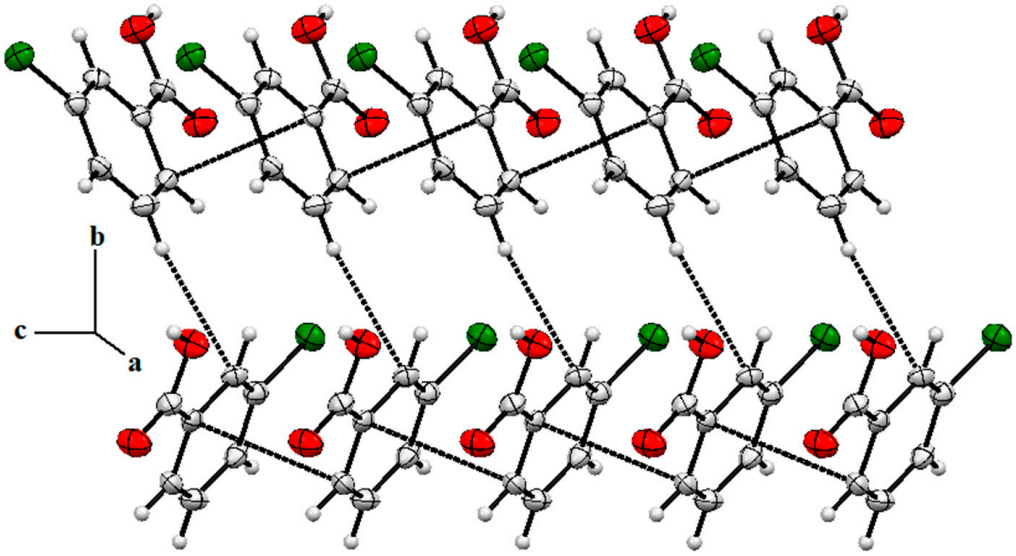

Figure 4. Acid-acid associations via π–π (C(1)---C(6)) and H(5)-π(C(2)) interactions, making a 2D network along the a and b axes.

2.5. Single X-ray of Compound **2** *(2-Amino-4-Chloropyridinium 3-Chlorobenzoate)*

A 1:1 acid/base unit of the molecule of compound **2** (monoclinic, space group $P2_1$) is shown in Figure 5 with a partial numbering scheme. The NH_2 group in the base is at appropriate position to afford an $R_2^2(8)$ loop, as has been observed in 2-aminopridine derivatives [38]. Here, the incorporation of a chloride function in the base was expected to adversely affect the basicity of ring N to hinder it from accepting H^+. Based on the difference in the pH of the pair, a cocrystal was anticipated, but the actual product was a molecular salt. It indicates the role of the structure of the acid/base unit in the co-crystal/molecular salt formation and not only the *p*H. The C(1)-O(1) and C(1)-O(2) distances in the acid are 1.264(5) and 1.247(6) Å, which reveal a difference in bond order between the C and oxygen atoms. Hydrogen bonding between O(1)---HN(1) link acid/base pairs, with a distance

between O and H of 1.998 Å, making a stronger interaction when compared with the H-bonding in compound **1**. As a result of this interaction, acid/base pairs extend in 1D fashion along the b-axis, as shown in Figure 6 (left). Among short contacts, C(1)---C(8), C(11)---O(2), and C(11)---H(3) are linked together with distances of 3.376, 3.165, and 2.832 Å, respectively. These short interactions stabilize the supramolecular structure along the b and c axes, as shown in Figure 6 (right).

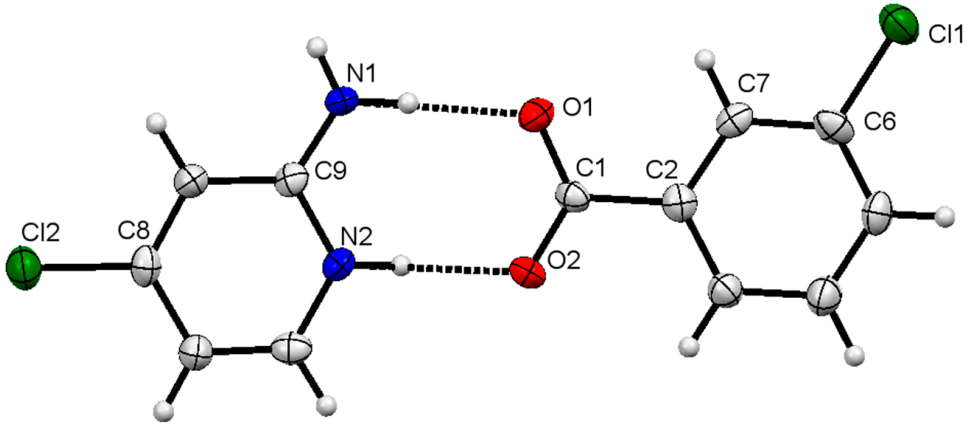

Figure 5. Molecular unit of compound **2**, with a partial numbering scheme; thermal ellipsoids are drawn at a 50% probability level. Proton transfer in the molecule is clear, and the acid–base pair makes an $R_2^2(8)$ loop.

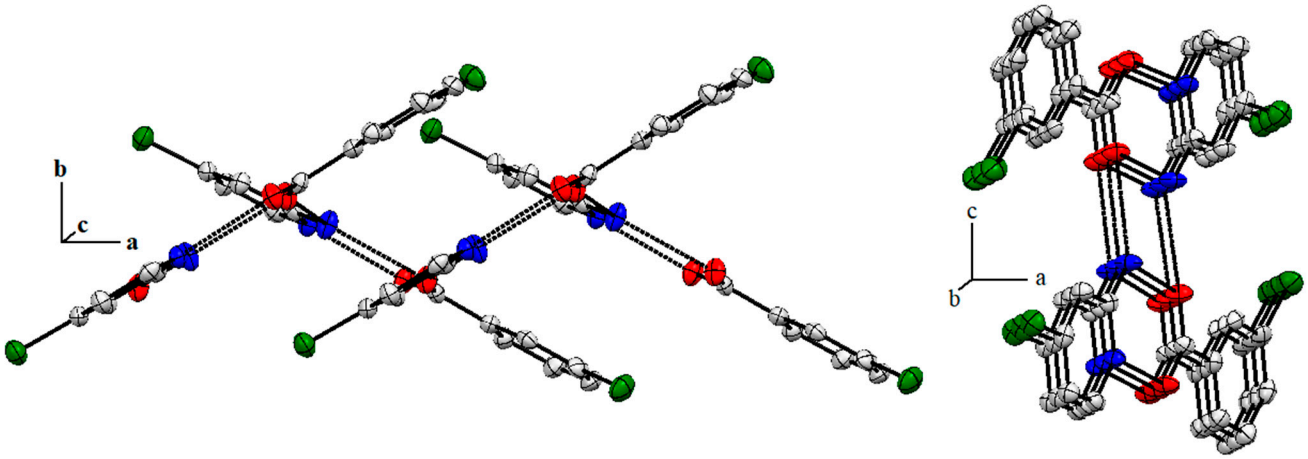

Figure 6. Two-dimensional structure of the compound stabilized via short-range interactions (**left**); the molecules of compound **2** associated via H-bonding (**right**); contacts are deleted for clarity. In both structures, hanging contacts are deleted for clarity.

2.6. Structure Description of Compound **3** *(2-Amino-4-Chloropyridinium 4-Chlorobenzoate)*

The crystalline nature of compound **3** is monoclinic with the space group *P*c. Its molecular structure is shown in Figure 7 with a partial numbering scheme. The oxygen atoms of the compound suffer from slight disorder in which the data pertaining to structural features such as bond lengths can be misleading. The structure provides enough information to establish the proposed connectivity of an acid/base pair like compound **2**. The structure indicates that proton transfer takes place from the acid to the base in a similar way as discussed for compound **2** to afford a molecular salt, making the ring system $R_2^2(8)$. Proton transfer is evident from the difference in the C-O bond length in the COO group. The C(7)-O(1) and C(7)-O(2) bond lengths are 1.658(19) and 1.072(19) Å. The electron density is localized within the C=O bond rather than delocalized along the O-C-O fragment. The acid/base pair is coplanar, with negligible deviation from planarity. Both coformers are linked with the help of H-bonding where distance between O(2) and N(2) is relatively short

(2.518 Å) as compared to compound **2**. As discussed above, the disordered O(1) interacts with N(1)H with separation distances of 1.689 (O(1)---H) and 2.529 Å (O(1)---N(2)). The O(1) and N(2) are potential centers for H-bonding, and they interact with neighboring salt molecules, stabilizing a 1D straight chain (Figure 8).

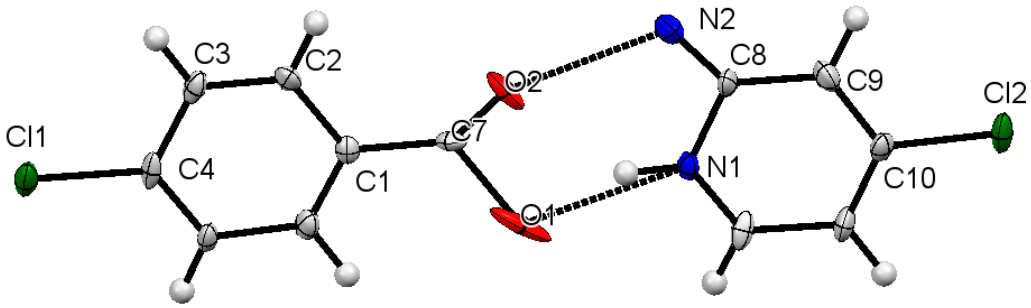

Figure 7. Solid state structure of a 1:1 molecular salt of 4-chlorobenzoic acid:2-Amino-4-chloropridine, compound **3**.

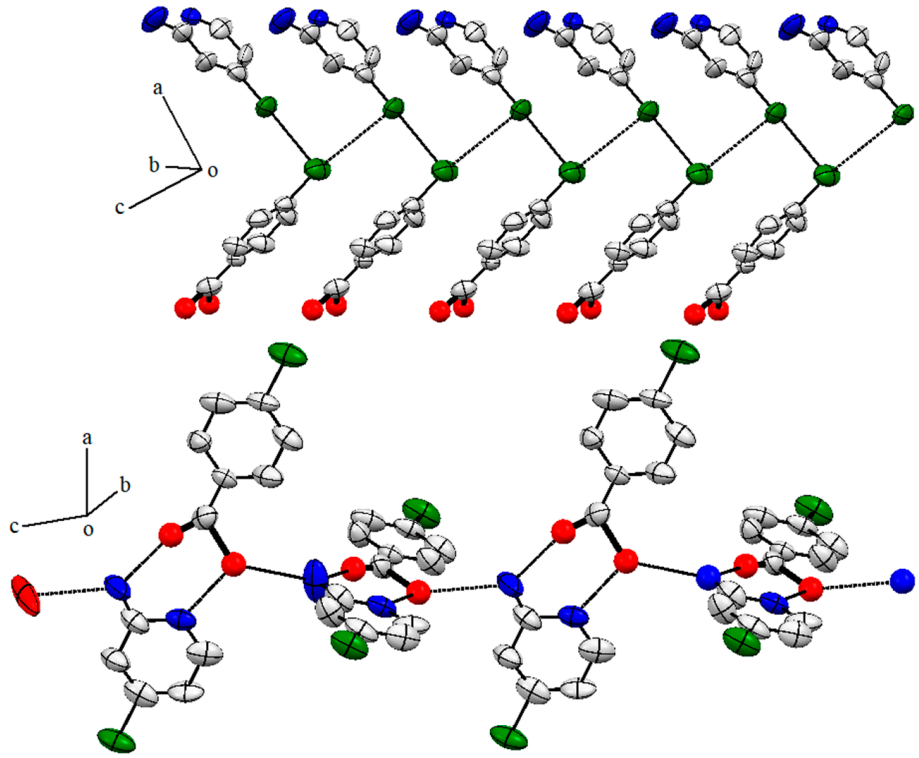

Figure 8. One-dimensional ((**lower**), along c-axis) and partial three-dimensional (**upper**) extensions of the molecules of compound **3**, stabilized by H-bonding and short contacts including Cl---Cl interactions, respectively.

An overview of short contacts indicates that Cl---Cl interactions are present in the molecules. The acid moiety through Cl(1) links two base synthons through Cl(2) and similarly, each Cl(2) interacts with two Cl(1). The distance between Cl(1) and Cl(2) is slightly different due to different orientations of the molecules in the space, i.e., 3.453 and 3.461 Å (Figure 9). Other types of short contacts were not observed in the molecules of compound **3**.

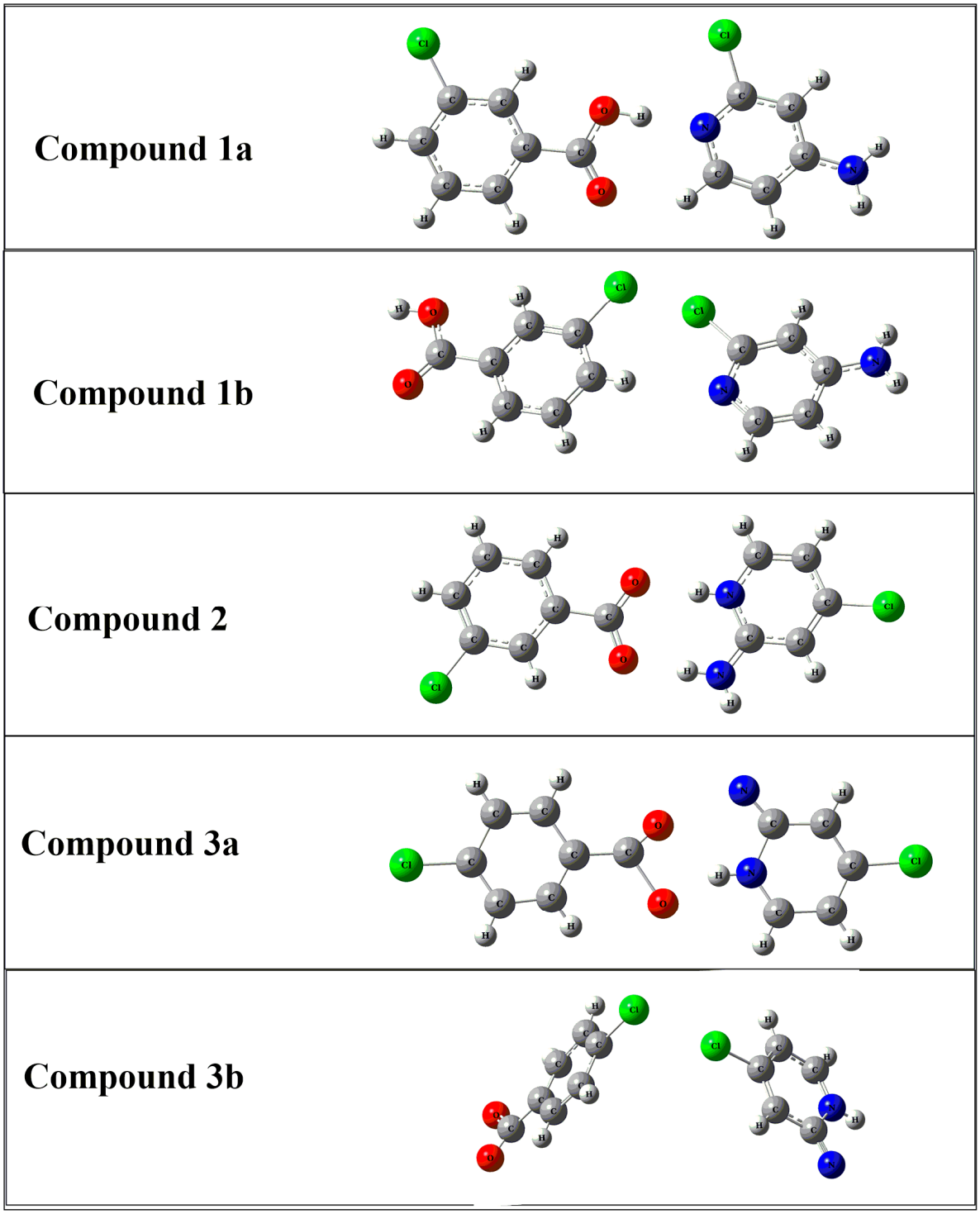

Figure 9. Dimers of compounds **1**–**3**, calculated via the B3LYP-D3/6-311++G(d,p) method.

3. Supramolecular Interactions via DFT Calculations

DFT studies of compounds **1**–**3** were performed to analyze insights into supramolecular assemblies in a solid state, and relaxed geometries are given in Figure 9. Important nonbonding interactions such as hydrogen bonding, halogen bonding, and van der Waals interactions are prominent in crystal packing. Such interactions were also observed in optimized gaseous-phase structures of all these compounds (**1**–**3**). In the crystal structures of compounds **1** and **3**, hydrogen bonding as well as halogen bonding can be seen between acid–base pairs on opposite sites. To examine such interactions [53–55], two types of orien-

tations were considered for the dimeric compounds **1** (**1a** for hydrogen bonding and **1b** for halogen bonding) and **3** (**3a** for hydrogen bonding and **3b** for halogen bonding). These compounds (**1a**, **1b**, **2**, **3a**, and **3b**) were optimized at the same B3LYP-D3/6-311++G(d,p) level of theory. As a result of these interactions, thermodynamically stable clusters were formed. Thermodynamic stability was confirmed using the counterpoise-corrected energies (E_{cp}) and interaction energies (E_{int}) of these compounds (**1–3**), and the values are given in Table 1. The E_{cp} values of dimers of the compounds **1a**, **1b**, **2**, **3a**, and **3b** are −12.91, −2.10, −96.45, 36.37, and 52.63 kcal/mol, respectively. The highest E_{cp} (−96.45 kcal/mol) is seen for compound **2**, and the lowest E_{cp} (−2.10 kcal/mol) is obtained for compound **1b**. The negative signs represent the feasibility of dimerization; ultimately, all the reactions are exothermic in nature except compounds **3a** and **3b**, which show endothermic behavior. The hydrogen-bonded dimers (**1a**, **2**, and **3a**) are more stable compared to the halogen-bonded dimers (**1b** and **3b**). The E_{int} values of dimers of the compounds **1a**, **1b**, **2**, **3a**, and **3b** are −17.81, −8.20, −101.32, −29.99, and −46.12 kcal/mol, respectively. The E_{int} values of the respective dimers are comparable to the E_{cp} values, which agrees with previously reported similar work on complexation of different chemical species [56]. Compounds **1a** and **1b** are neutral species, whereas compounds **2**, **3a**, and **3b** are charged species. In the case of compound **2**, electrostatic interactions are responsible for strong interactions. In compounds **1a** and **1b**, hydrogen and halogen bonding play dominant roles. Compounds **3a** and **3b** also show weak electrostatic intaeractions compared to other compounds.

3.1. Frontier Molecular Orbital (MO) Analysis

A frontier molecular orbital (MO) analysis was performed to evaluate the electronic properties of compounds **1–3**. During this analysis, the energies of the highest occupied molecular orbitals (E_{HOMO}), the lowest unoccupied molecular orbitals (E_{LUMO}), and the HOMO-LUMO gap ($E_{L\text{-}H}$) were calculated. The E_{HOMO} values of compounds **1a**, **1b**, **2**, **3a**, and **3b** are −6.76, −6.72, −6.10, −5.93, and −5.82 eV, respectively. The E_{LUMO} values of compounds **1a**, **1b**, **2**, **3a** and **3b** are −1.38 eV, −1.72 eV, −3.01 eV, −0.47, and −0.65 eV respectively. The $E_{L\text{-}H}$ gaps of compounds **1a**, **1b**, **2**, **3a**, and **3b** were 5.38, 5.00, 3.09, 5.46, and 5.17 eV, respectively (Table 2). These values reflect the semiconductor behavior of these compounds, along with high chemical and kinetic stabilities. The same type of behavior was noticed in compounds recently reported in [57]. Electronic density distributions illustrate that in compounds **1a** and **1b**, the HOMO densities reside on the chloro-group of the 3-chlorobenzoic acid fragment and its nearest carbon (Figure 10). The reason is the electron-withdrawing effect of the halogen. The electronic densities of the LUMOs are localized on the acetate group and the carbon connected to this group. Partially, the densities also reside on the C-C bonds of the benzene ring, which is away from the chloro-group. Similarly, in compound **2**, the HOMO densities reside on the chloro-group of the 3-chlorobenzoic acid fragment. Some of the densities are also found on the carbon atoms attached to this group. The LUMO densities reside on the acetate group of the 3-chlorobenzoic acid fragment. Some of the densities are also found on the carbon–carbon bond attached to the acetate group. The reason might be because of the hydrogen transfer between the acetate group of the 3-chlorobenzoic acid and the amino group of the 2-amino-4-chloropyridine. Like compound **1**, the HOMO densities are localized on all atoms of the 2-amino-4-chloropridine except the chloro-group. The LUMO densities in compound **3a** are localized on the amino-group and the carbon–carbon bonds of 2-amino-4-chloropyridine. This is due to the fact that a strong noncovalent interaction exists between the amino group of 2-amino-4-chloropyridine and the oxygen atom of the acetate group in compound **3a**. Some of the density also resides on the oxygen atoms of the 4-chlorobenzoic acid. The HOMO densities are localized on the acetate group of the 3-chlorobenzoic acid fragment in compound **3b**. The LUMO densities are localized on the amino group and carbon–carbon bonds of the 2-amino-4-chloropyridine.

Table 2. Interaction energies (E_{int}), counterpoise-corrected energies (E_{cp}), and the energies of the highest occupied molecular orbitals (E_{HOMO}) and the lowest unoccupied molecular orbitals (E_{LUMO}) and the HOMO-LUMO gaps (E_{L-H}) of compounds **1–3**.

Compounds	E_{int}	Ecp	E_{LUMO}	E_{HOMO}	E_{L-H}
1a	−17.81	−12.91	−1.38	−6.76	5.38
1b	−8.20	−2.10	−1.72	−6.72	5.00
2	−101.32	−96.45	−3.01	−6.10	3.09
3a	29.99	36.37	−0.47	−5.93	5.46
3b	46.12	52.63	−0.65	−5.82	5.17

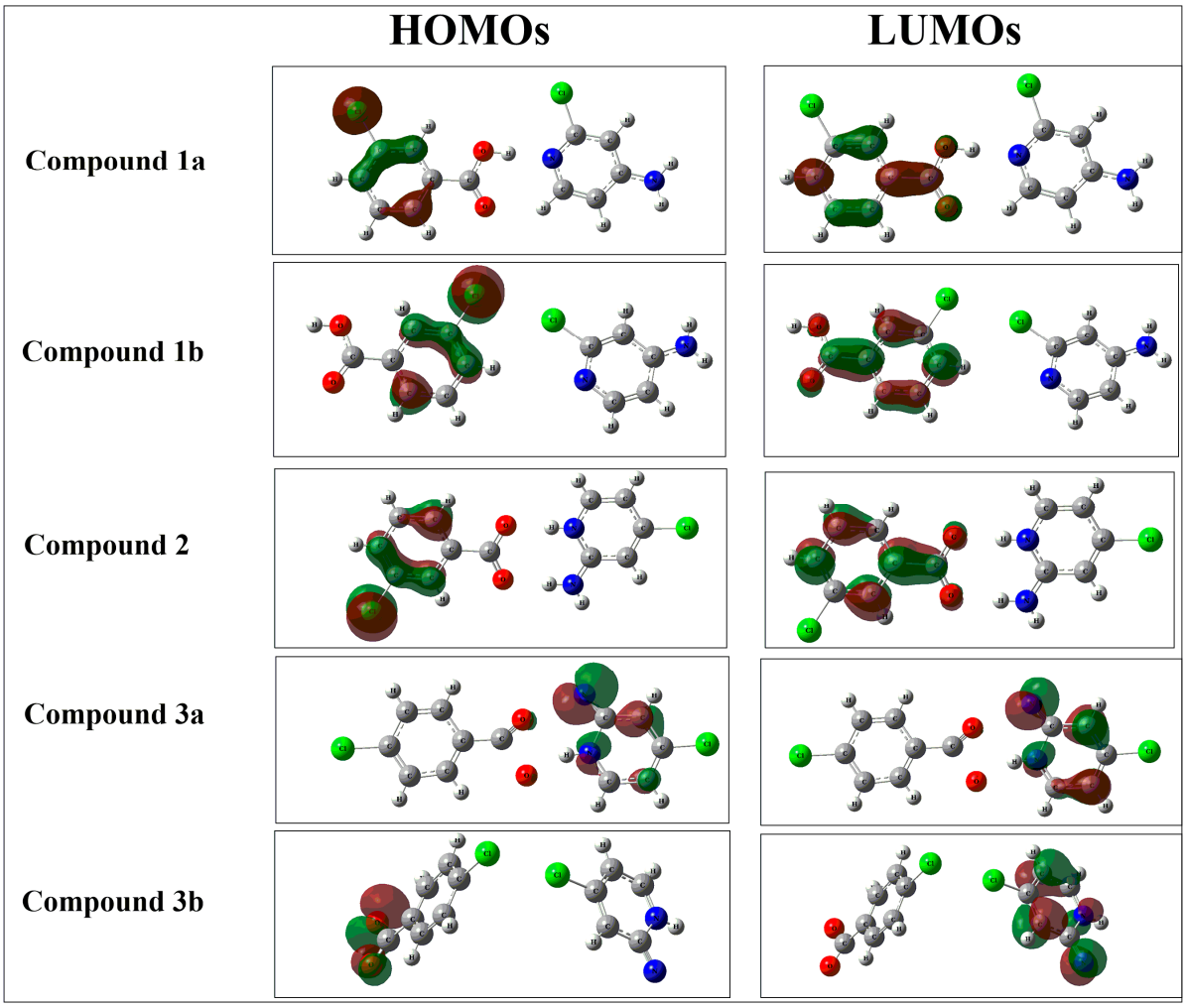

Figure 10. The isodensities of the highest occupied (HOMOs, green) and the lowest unoccupied molecular (LUMOs, dark red) orbitals of compounds **1–3**.

3.2. Molecular Electrostatic Potential (MEP) Analysis

A molecular electrostatic potential (MEP) analysis can be used for the prediction of reactive site compounds. The potentials on the surfaces of complexes are represented by different colors. The increasing order of electrophilicity is given as red < orange < yellow < green < blue. This range represents that the blue color shows electrophilic sites and red color shows nucleophilic sites. The green color surface depicts a neutral region of the respective compound [56]. To investigate these active sites in isolated organic acids and bases used for the synthesis of our compounds (**1a**, **1b**, **2**, **3a** and **3b**), the MEP surfaces of the acids and bases were constructed as shown in Figure 11. The red surfaces, seen on the oxygen atoms of the acetate groups in each of the organic acids, represent nucleophilic sites. On the other hand, the hydrogen of the

hydroxyl group in the organic acid shows an electrophilic site. The blue surfaces seen on amino groups reflect electrophilic sites in organic bases, and the nitrogen in the ring with a red surface indicates a nucleophilic site.

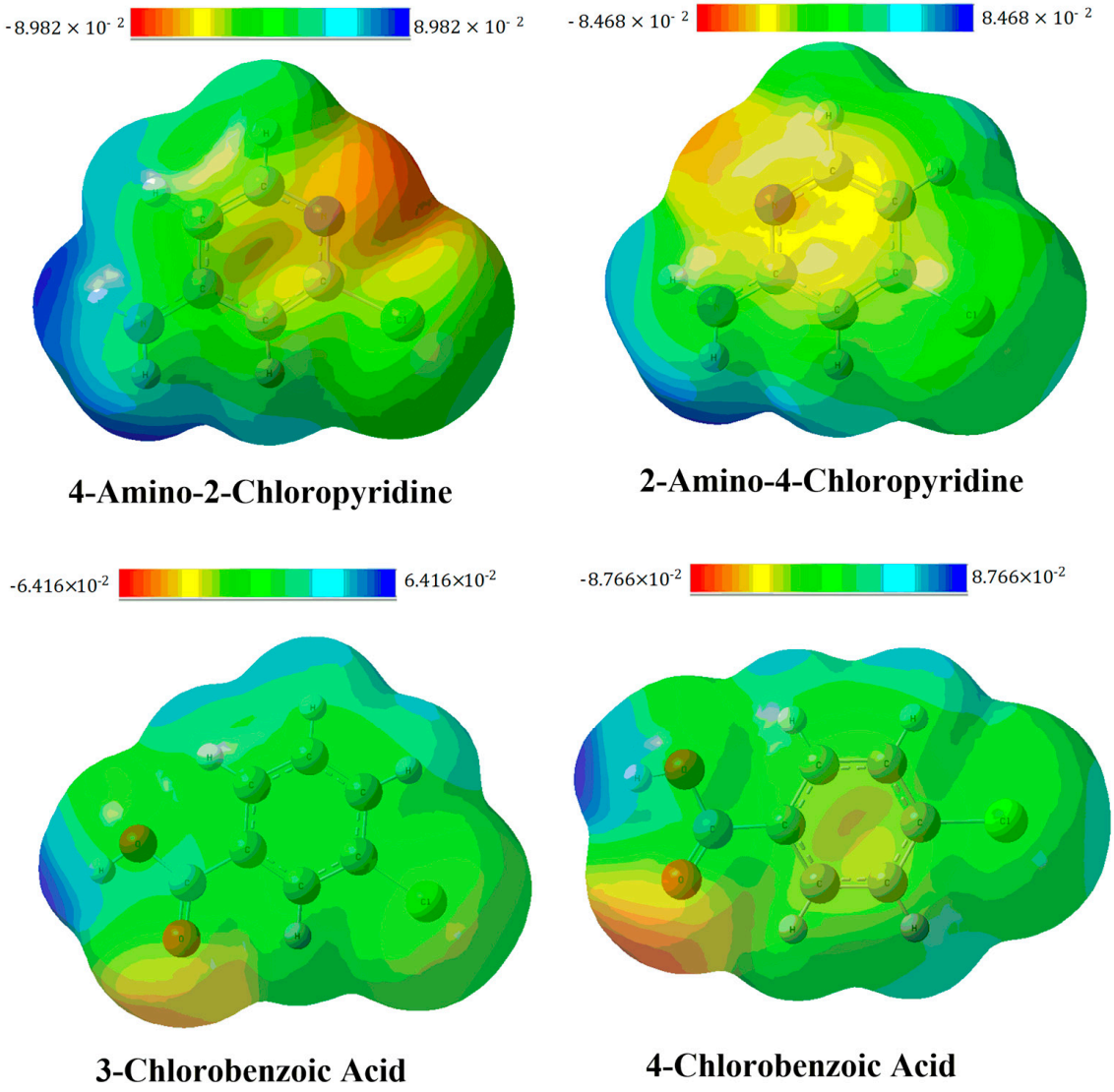

Figure 11. The molecular electrostatic potentials (MEPsr) of organic acids and bases.

Non-covalent interactions are also explained through sigma holes. These holes represent regions of lower electronic density (maxima) on the surface of a covalently bonded atom (along the extension of the bond), illustrating the anisotropies of atoms bonded through a covalent bond. In the region of these covalently bonded atoms, a positive electrostatic potential is generated, and the sites with these potentials are responsible for the interaction of the molecule with the negative sites (i.e., atoms with lone pairs of electrons, anions, and pi electrons) of another molecule. These holes are responsible for self-assembly in crystal growth through noncovalent interactions [58]. Contrary to sigma holes, regions of higher electronic density (minima) are also generated on the atoms with a negative electrostatic potential. Molecules can easily interact with positive sites through these negative potential sites [59]. In compounds **1–3**, sigma holes are generated on the hydrogen atoms of the amino group, which are responsible for hydrogen-bonding with a nucleophile during crystal growth. The energies of the maxima points are 52.19 and 51.72 kcal/mol for the hydrogens of the amino group, while the nitrogen of pyridine has a critical point energy of −30.51 kcal/mol.

In addition to amino groups, sigma holes are seen in chloro-groups in compounds **1–3**, which are responsible for halogen bonding during crystal growth. The chloro-group acts as an electrophilic site for the incoming nucleophile (Figure 12). The positive potentials on the chloro-group of the pyridine ring have maximum energies of approximately 35.65 kcal/mol. For 3-chlorobenzoic acid and 4-chlorobenzoic acid, the oxygen atoms of the carbonyl groups have minimum points on the global energy surface with energies of −30.81 and −30.50 kcal/mol, respectively. These sites act as nucleophiles and have negative potential due to the presence of lone pairs of electrons of the oxygen atoms in the carbonyl group. Thus, the hydroxyl site acts as an electrophilic site, and oxygen acts as a nucleophilic site. Overall, benzoic acid moieties withdraw electron density from pyridine in complexation, leaving it electron-deficient in all compounds **1–3**. The most prominent sigma hole is seen in compound **2**. The greater polarizability of the bonds between benzoic acid and pyridine moieties causes an increase in the electropositive regions of the sigma holes, resulting in stronger non-covalent interactions. In addition to polarizability, the strong electron-withdrawing group in benzoic acid increases the positive potential on the chlorine group of the pyridine moiety, strengthening the noncovalent interactions. The presence of sigma holes in our compounds confirms the occurrence of noncovalent interactions in compounds **1–3**.

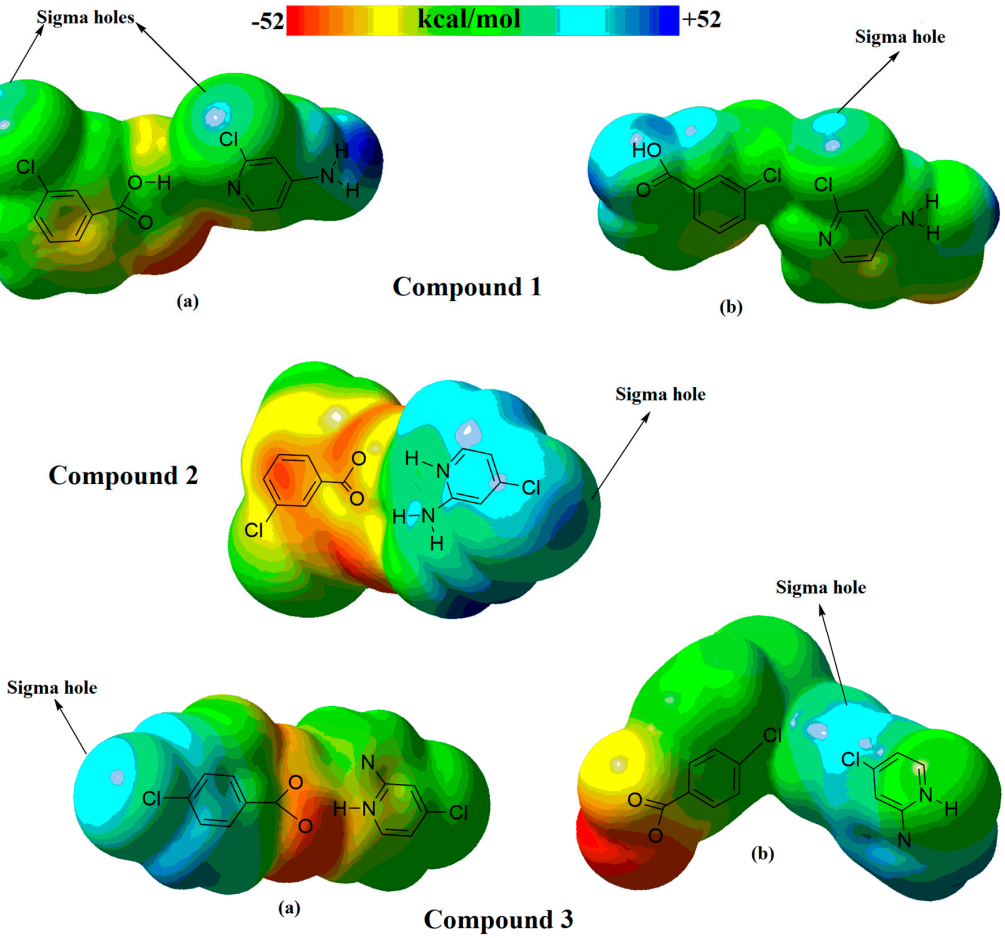

Figure 12. Graphical representation of prototypical sigma hole related to halogen bonding in compounds **1–3**. Blue and red colours represent electropositive and electronegative regions, respectively, Different orientations of molecules of compounds **1** and **3** are shown as (**a**,**b**) for better visualization of sigma holes.

3.3. Noncovalent Interaction (NCI) Analysis

For a further deep visualization of noncovalent interactions, an NCI analysis was carried out. Noncovalent interactions including weak Van der Waals interactions, hydrogen bonding,

and steric repulsion were studied as observed in real space [56]. Three-dimensional NCI isosurfaces and two-dimensional reduced density gradient (RDG) graphs were constructed, and data are given in Figure 13. In the three-dimensional NCI plots, the nature of different interactions is estimated from three different colours of the isosurfaces [60]. Strong hydrogen-bonding (HB) and weak London dispersion interactions (LDI) are observed as blue and green isosurfaces, respectively. Repulsive interactions (RI) appear in red between interacting monomers of a complex. Moreover, the strength and intensity of the interactive forces are proportional to the thickness of the isosurfaces. The NCI plots represent electrostatic and hydrogen bonding between the benzoic-acid- and amino-pyridine-containing fragments in each of these compounds (**1a**, **1b**, **2**, **3a**, and **3b**). But hydrogen bonding is a dominating interaction in all compounds **1a**, **2**, and **3a**, whereas halogen bonding (Cl-Cl) is the dominant interaction in compounds **1b** and **3b**. The thickness of the isosurfaces represents strong interactions between two fragments which justify the stability of all these compounds.

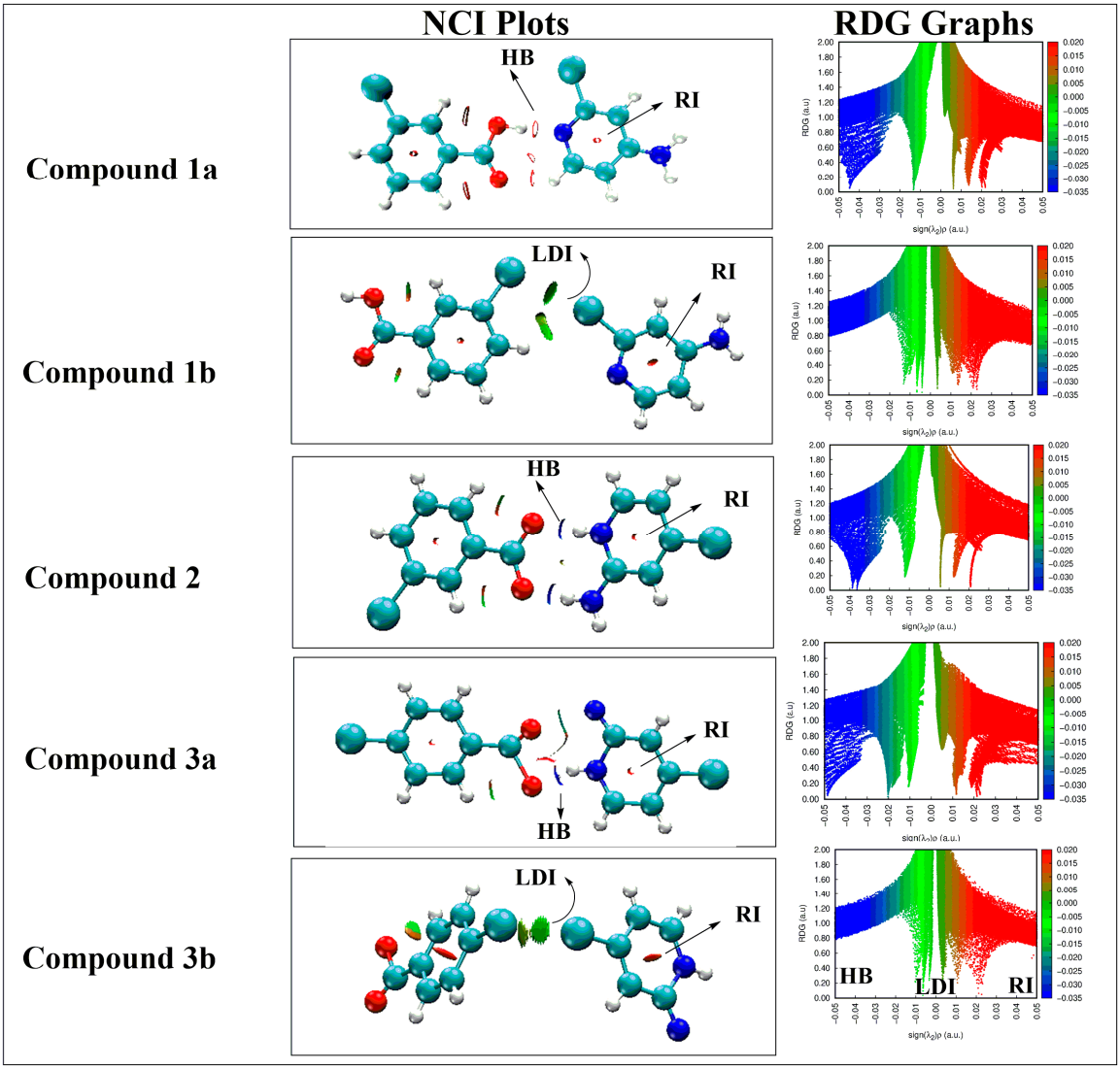

Figure 13. The 3D noncovalent interactions (NCI plots) and 2D reduced density gradient (RDG) graphs of compounds **1**–**3**. The three types of interactions, hydrogen bonding (HB), London dispersion interaction (LDI), and repulsive interactions (RI), are represented by blue, green, and red, respectively.

In the two-dimensional RDG graphs, the sign $(\lambda_2)\rho$ values are in the range of 0.05 to −0.05 au in scatter graphs which exhibit three types of interactions including hydrogen bonding, weak van der Waals forces, and repulsive forces. Various spikes appeared in these graphs, with blue, green, and red colors for strong van der Waals forces (such as hydrogen

bonding), weak van der Waals forces, and repulsive forces, respectively. Furthermore, the deep RDG spikes and more negative $(\lambda_2)\rho$ values (−0.03 to −0.05 au) of spikes reflect the presence of strong hydrogen bonding in compounds **2**, **1a**, and **3a**, respectively. Blue patches are absent in this region, but a few blue spikes in isosurfaces are obtained in the $(\lambda_2)\rho$ region of −0.02 to −0.03 au. In addition to blue, green color spikes in the 0.01 to −0.01 au range represent weak van der Waals interactions in all compounds **1**–**3** but are more prominent in **1b** and **3b**. The dark red-green spikes between the 0.00 and 0.01 au regions in the RDG graphs of compounds **1**–**3** represent C-H---π interactions between two fragments. The red spikes in the 0.02 to 0.03 au regions of the RDG graphs reflect repulsive forces between the two fragments in each of the five compounds **1**–**3**. These blue, red, and green spikes indicate the presence of hydrogen, weak van der Waals, and electrostatic repulsive interactions.

3.4. DFT Studies for Clusters of Compounds **1**–**3**

The large clusters of compounds **1**–**3** were also modeled (in the orientations obtained from their crystal structures) and optimized at the same B3LYP-D3/6-311++G(d,p) level of theory (Figure 14). For compound **1**, two types of orientations are considered, one in which halogen bonding is prominent and a second in which hydrogen bonding is seen. These two types of orientations are named compound **1**-hydrogen bonding and compound **1** halogen-bonding (Figure 14). All these clusters are thermodynamically highly stable, as is evident from their interaction energies which illustrate that all reactions are exothermic in nature and that the cluster formation of these compounds is highly feasible. The HOMO and LUMO densities were also constructed, and it can be observed that localizations of densities on fragments are similar to the initial dimeric compounds **1**–**3**. The HOMO densities are localized on the acetate group of the benzoic-acid-containing fragment, and the LUMOs reside on the amino-pyridine fragment in all packing clusters of **1**–**3**. Furthermore, MEP surfaces were also constructed on all four trimeric compounds **1**–**3**. Similar to the isolated dimeric compounds **1**–**3**, again, the amino group represents an electrophilic site, whereas the acetate groups represent nucleophilic sites as we observe a red color on acetate groups and a blue color on amino groups, respectively. The chloro-groups seem to have neutral behavior which is evident from the green color on the MEP surfaces.

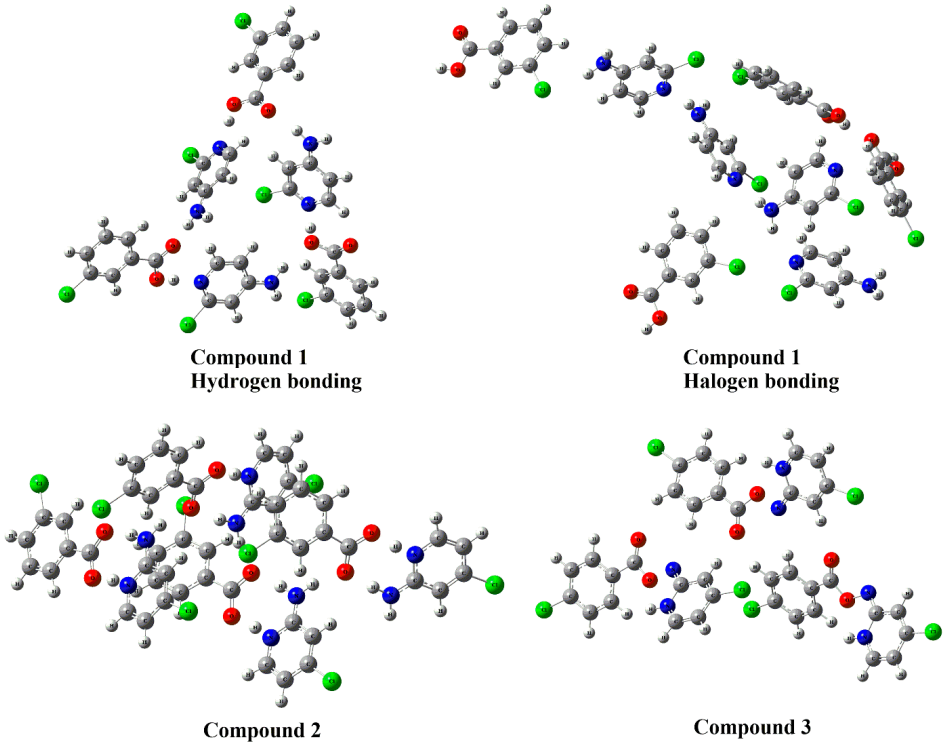

Figure 14. The clusters of compounds **1**–**3**, calculated using the B3LYP-D3/6-311++G(d,p) method.

NCI plots and RDG graphs were also constructed for clusters of compounds **1–3** (Figure S9 and Supporting Information Figure S4). The NCI plots represent electrostatic and hydrogen bonding between the two benzoic-acid- and amino-pyridine-containing fragments in each of the trimeric compounds **1–3**. But hydrogen bonding is the dominating interaction in all three trimeric compounds **1–3**. The thickness of the green isosurfaces represents strong interactions between the two fragments which justifies the stability of all these compounds. The blue, red, and green spikes in the RDG graphs of clusters of **1–3** (Figure 13) indicate the presence of hydrogen, weak van der Waals, and electrostatic/repulsive interactions between different fragments of the compounds.

3.5. UV Absorbance Spectra

Compounds **1–3** were scanned in the UV/visible region between 200 and 800 nm with a fast scanning speed. The Beer–Lambert law was used for the determination of the molar extinction coefficient (ε) of each of the compounds. The results and molar absorptivity values are given in Table 3. For the determination of the molar absorptivity coefficient, measured absorbance maxima were divided by the sample concentrations for an optical path length of 1 cm. For obtaining UV-visible spectra, 0.5 μM solutions in methanol (cutoff value = 205 nm) were prepared in which the intensities of solvent blanks were noted at 0.014, 0.013, and 0.017 for **1–30**, respectively. The absorption intensities for compounds **1–3** were 0.39, 0.30, and 0.31, respectively, from which the molar absorptivity of each sample was calculated, as given in Table 3.

Table 3. UV/visible data of compounds **1–3**.

Compound	λ_{max}	Molar Absorptivity Coefficient (ε)
1	345 ± 1	782
2	243 ± 1.5	604
3	344 ± 1	632

4. Biological Applications of Compounds

4.1. Antioxidant Essay (DPPH)

Antioxidant materials are classified into different classes according to their mode of action, like chelators, free-radical scavengers, and oxygen scavengers. Several available methods exist to determine antioxidant activates. A DPPH free radical scavenging assay was used to evaluate the antioxidant potential of these compounds. 2-2-diphenyl-1-picrylhydrazal (DPPH) is a stable free radical and is commercially available. Mostly, compounds have been tested for free radical scavenging relative to of DPPH by following the method described in [61]. The method was followed with a slight modification for the determination of the DPPH free radical scavenging ability of the synthesized cocrystal and molecular salts and their coformers. As per the literature, DPPH absorbs UV light at 517 nm, but the absorption is dependent on the concentration of the solution (Figure S8). The central nitrogen accepts an electron or a hydrogen atom, resulting in decolorization from dark purple to yellow and then colorless, which can be measured using the decreasing absorbance in UV light.

A solution of DPPH was prepared in an ethanol/water (1:1, v/v) solvent system by dissolving 0.348 g of DPPH per 100 mL of solution. Various concentrations of solutions (50, 100, 150, 200, and 250 μg/mL) were prepared for both starting precursors and the synthesized compounds from a stock solution of each sample (0.001g in 10 mL). To each solution, 1 mL of DPPH was added and incubated for 30 min. Changes in color were observed from purple to yellow and then to colorless upon increasing the concentration. The IC_{50} values for DPPH free radical scavenging are given in Table 4. It is evident that the

molecular salts (**2** and **3**) are more efficient than the cocrystal (**1**). The percent inhibition values were determined using the below formula:

$$\%\text{Inhibition} = \frac{A_{control} - A_{sample}}{A_{control}} \times 100$$

Table 4. DPPH free radical scavenging efficiency of compounds **1**–**3** and their coformers, where ascorbic acid was used as standard.

Compounds	Conc. µg/mL	Sample	Control	%RSA	IC_{50}
3-Chlorobenzoic acid	50	0.355	0.52	31.73	4.85
	100	0.316		39.23	
	150	0.289		44.42	
	200	0.269		48.27	
	250	0.21		59.62	
4-Amino-2-chloropyridine	50	0.455	0.52	12.5	9.53
	100	0.436		16.15	
	150	0.399		23.27	
	200	0.389		25.19	
	250	0.28		46.15	
2-Amino-4-chloropyridine	50	0.45	0.52	13.46	8.27
	100	0.416		20	
	150	0.369		29.04	
	200	0.315		39.42	
	250	0.26		50	
1	50	0.35	0.52	32.69	4.92
	100	0.32		38.46	
	150	0.29		44.23	
	200	0.26		50	
	250	0.21		59.62	
2	50	0.31	0.52	40.38	4.05
	100	0.28		46.15	
	150	0.24		53.85	
	200	0.21		59.62	
	250	0.18		65.38	
3	50	0.31	0.52	40.38	3.55
	100	0.29		44.23	
	150	0.26		50	
	200	0.22		57.69	
	250	0.21		59.62	

4.2. Anti-Bacterial Study of Compounds **1**, **2** *and* **3** *and Their Comparison with Coformers*

One of the best available strategies to enhance anti-bacterial efficiency and other properties of compounds are salt/cocrystal formulations. For enhancing the in vitro anti-bacterial activities of pharmaceutical drugs, this strategy is very efficient [62]. The antibacterial activity and zones of inhibition of the synthesized compounds and their coformers were determined against both Gram-positive and Gram-negative bacteria. *Staphylococus aureus* and *Staphylococcus epidermis* are Gram-positive, while *Klebsiella pneumonia* and *Pneumonia mirabilis* are Gram-negative bacteria. From the average zone of inhibition, it is evident that the cocrystal and salt formulations both increase antibacterial activity. Compounds **2** and **3** show efficient anti-bacterial activity over compound **1** (cocrystal) against both Gram-positive and Gram-negative bacterial strains. The coformers of the compounds are less efficient compared to their respective heterosynthons against the selected bacterial strains (Table 5).

Table 5. Anti-bacterial study of compounds **1**–**3** and their comparison with coformers.

Compound No.	Average Zone of Inhibition (mm)											
	Gram Positive						Gram Negative					
	S. Aureus			*S. Epidermis*			*K. Pneumonia*			*P. Mirabilis*		
	Acid	**Base**	**Product**	**Acid**	**Base**	**Product**	**Acid**	**Base**	**Product**	**Acid**	**Base**	**Product**
1	12	10	14	11	18	13	11	06	16	11	14	13
2	12	09	16	11	08	14	11	05	17	11	07	14
3	11	09	15	10	08	14	15	05	16	13	07	15
Standard Azithromycin		28			27			30			27	

5. Materials and Methods

5.1. General Considerations and Instrumentations

The benzoic acid and pyridine derivatives used in this study were depicted in Scheme 1 above. Chemicals, 3-chlorobenzoic acid, 4-chlorobenzoic acid, 2-amino-4-chloropyridine, and 4-amino-2-chloropyridine, were purchased from TCI, Japan, and were used as received. Melting points, uncorrected, were determined with the help of Stuart SMP-10, Japan. The melting points of the final products were compared with their respective coformers (157 ± 1 °C (3-chlorobenzoic acid), 241 ± 1 °C (4-chlorobenzoic acid), 153 ± 1 °C (4-amino-2-chloropyridine), and 126 ± 1 °C (2-amino-4-chloropyridine)); the difference in values was taken as a positive sign of a successful reaction. The FT-IR spectra of the resultant compounds were recorded using a SHIMADZU FT-IR Model 18,400, and single X-ray diffraction data were collected with the help of a Bruker D8 VENTURE diffractometer with a PHOTON II detector and dual-wavelength Mo/Cu and Mo-Kα, λ = 0.71073 Å. Cell refinement and data reduction were carried out using SAINT V7.06A software [63]. The crystal structure solution and refinements were accomplished using SIR97, [64] SHELXL97, [65] WinGX31 [66], and PLATON [67].

5.2. Synthesis of Compound **1**, *(Cocrystal of 3-Chlorobenzoic Acid:4-Amino-2-Chloropyridine)*

The solution of 3-chlorobenzoic acid (0.1 g; 0.638 mmol) was prepared in 5 mL of acetonitrile. The acid solution was added dropwise to a separately prepared solution of 4-amino-2-chloropyridine (0.08 g; 0.638 mmol). The reaction was executed according to the reported procedure in [38]. The mixture of both coformers was refluxed for 4 h with constant stirring at ca. 300 rpm. The solution mixture was stored and placed for slow evaporation; after few days, transparent (white) crystals appeared. The crystals were isolated from the mother liquor and studied (m. p. = 110–112 °C; FT-IR data, ν (cm^{-1}) = 3773, 3144, 3000, 2919, 2820, 2170, 1980, 1720, 1632, 1450, 1344).

*5.3. Synthesis of 2-Amino-4-Chloropyridinium 3-Chlorobenzoate (***2***) and 2-Amino-4-Chloropyridinium 4-Chlorobenzoate (***3***)*

Molecular salts **2** and **3** were prepared under reflux conditions using equimolar ratios (1:1) of acids and bases. Solution of 3-Chlorobenzoic acid (for compound **2**), 4-chlrobenzoic acid (for compound **3**) (0.1 g; 0.063 mmol each), and 2-amino-4-chloropyrdine (0.082 g; 0.063 mmol) were separately prepared in acetonitrile. The acid–base solutions were slowly mixed, and the reactions were processed as discussed for compound **1**. The crystals of both compounds were grown in the same solution at room temperature via slow evaporation. The melting points of the starting precursors/coformers are 157 ± 1 °C (3-chlorobenzoic acid), 241 ± 1 °C (4-chlorobenzoic acid), and 126 °C (2-amino-4-chloropyridine).

Compound **2**: m. p. = 210–211 °C; FT-IR data, ν (cm^{-1}) = 3750, 3355, 3134, 3090, 2960, 2940, 2790, 1728, 1640, 1580, 1400, 1330, 1021, 798, 712.

Compound **3**: m. p. = 180–182 °C; FT-IR data, ν (cm^{-1}) = 3700, 3080, 3043, 2944, 2910, 2840, 1740, 1600, 1580, 1540, 1400, 1180, 810, 760.

5.4. Computational Methodology

All required simulations were performed using Gaussian 09 software [68], and the results were visualized using GaussView 05 software [69]. A B3LYP-D3 with 6-311++G(d,p) basis set was used for the computational modeling of compounds **1**–**3**. B3LYP better explains the geometry of a system, and D3 was added to study the dispersion forces inside the designed structures. The larger basis set was used in this study due to the fact that the geometries and energies of systems are sensitive to basis sets. A higher basis set provides more accurate results for a desired data set than a lower basis set [70]. After structure elucidation, a frontier molecular orbital (FMO) analysis was also performed.

Molecular electrostatic potential was analyzed at the same level of theory (B3LYP-D3/6-311++G(d,p)), providing information about electrophilic and nucleophilic sites [70]. The thermodynamic stability of the compounds was estimated using interaction energies (E_{int}). This interaction energy was corrected for basis set superposition error (BSSE) [71]. Whenever two isolated molecules interact through van der Waals forces, the basis functions of one molecule interact with those of the other, resulting in BSS. This error was corrected using the Bernardi and Boys method of counterpoise correction (CP). In this method, counterpoise-corrected energies (E_{cp}) are calculated by subtracting BSSE energies from the E_{int}. The energies of the lowest unoccupied molecular orbitals (E_L), the energies of the highest occupied molecular orbitals (E_H), and the energy gap between these two orbitals ($E_{L\text{-}H}$) were also calculated at the same level of DFT. These data were used to obtain information about the stability of the compounds. Noncovalent interaction (NCI) plots and RDG graphs were constructed using MultiWfn V3.80 software [59] that provide detailed information related to noncovalent interactions between the individual monomers of compounds (**1**–**3**) and also between trimers of all compounds (**1**–**3**) [72].

5.5. In Vitro Antibacterial Study

Following the reported procedure, an agar solution and Petri dishes were sterilized in an autoclave [73,74]. About 20 mL of sterile agar solution was added to each Petri dish, followed by incubation at 37 °C for 24 h. After incubation, the plates were inspected, and the contamination-free plates were selected for further study. The bacterial strains (*S. Epidermis*, *P. Mirabilis*, *S. aureus,* and *K. pneumonia*) were carefully spread with the help of sterile swabs on the surfaces of the agar plates. Standard azithromycin and an equivalent amount of synthesized material (500 µg/mL) were dissolved to prepare a solution. A volume of about 5 µL from each solution was added to 6 mm disk filter paper. The sample-loaded disk filters were kept at a certain distance on the surfaces of the inoculated agar plates and then incubated at 37 °C for 24 h. After incubation, the zone of inhibition values were noted manually.

5.6. Determination of Antioxidant Potential

The 2,2-diphenyl-1-picrylhydrazyl (DPPH) assay was used to determine the antioxidant potential (free radical scavenging activity) of the prepared materials and the respective pure starting materials [57]. Samples of about 20 µL and a DPPH reagent volume of 180 µL were loaded into microplate wells. Afterwards, the samples were incubated for 1 h. Ascorbic acid was used as a positive control at different concentrations (0.75, 1.5, 3, 6, and 15 µg/mL). The absorbance of each sample and control were recorded using a Uv-Visible spectrophotometer. All experiments were performed in triplicate, and the results were obtained as the average of three readings. The percentage of free radical scavenging activity was calculated using the following equation [75]:

$$Percent\ inhibition = \frac{Control\ absorbance\ -\ sample\ absorbance}{Control\ absorbance} \times 100$$

6. Conclusions

In this study, the chemical reagents 3-chlorobenzoic acid and 4-amino-2-chloropyridine and 4-chlorobenzoic acid with 2-amino-4-chloropyridine were treated for the formulation of multicomponent structures. The differences in pH between the acids and bases in the respective pairs for compounds **1**, **2**, and **3** are 0.88, 1.87, and 1.74, respectively. The resultant materials were obtained as expected. For the acid/base pair in compound **1** (3-chlorobenzoic acid/4-amino-2-chloropyridine), a cocrystal was obtained, while compound **2** (3-chlorobenzoic acid/2-amino-4-chloropyridine) and **3** (4-chlorobenzoic acid/2-amino-4-chloropyridine) are molecular salts. Chlorine moieties at different positions in acids as well as in bases did not alter the formation of cocrystals or salts; however, they contributed to a minor extent to supramolecular chemistry. The products were characterized using FT-IR, PXRD, and SC-XRD analyses. The SC-XRD analysis clearly depicted that halogen bonding and hydrogen bonding played very important roles in the crystal design of the compounds. DFT studies provided evidence of the thermodynamic and electronic stabilities of the synthesized dimers (**1**–**3**) and their clusters. The highest E_{cp} (−96.45 kcal/mol) was observed for compound **2**, while the lowest E_{cp} (−2.10 kcal/mol) was obtained for compound **1b**. This study conclusively demonstrated the existence of weak noncovalent interactions between organic acids and bases which are responsible for their stabilities, as supported by an NCI analysis. Furthermore, noncovalent interactions confirm the presence of hydrogen bonding and halogen bonding. A MEP analysis offers detailed insights into the nucleophilicity and electrophilicity of the acetate and amino groups, respectively, during complexation. The DPPH free radical scavenging efficiency of compound **1** increases with an increase in concentration while in the case of compound **3**, a decrease occurred initially; then, it became independent of concentration. The antibacterial study shows that the cocrystal and molecular salts obtained in this study exhibited moderate efficiency. A mutual comparison of the three compounds (**1**, **2** and **3**) indicates that the molecular salts are relatively more active than the cocrystal against both Gram-positive and Gram-negative bacteria. These compounds are also more efficient than their respective starting precursors. The strategy of cocrystal or salt formation can lead to more efficient products for other derivatives.

Supplementary Materials: The following are available online at https://www.mdpi.com/article/10.3390/cryst13121663/s1. The following are the supplementary data for this article. Crystallographic data were deposited at the Cambridge Crystallographic Data Centre as Supplementary Publications no. 2117438-2117439 (Compounds **1** and **2**) and 2244702 (Compound **3**) Copies of the data can be obtained, free of charge, upon application to CCDC, 12 Union Road, Cambridge, CB2 1EZ, UK (fax: +44-1223-336033; e-mail: deposit@ccdc.cam.ac.uk). The supporting files contain FT-IR spectra (Figure S1: FT-IR spectra of compound **1** and its starting precursors (a) 3-chlorobenzoic acid, (b) 4-amino-2-chloropyridine, and (c) the 1:1 cocrystal of 3-chlorobenzoic acid:4-amino-2-chloropyridine; Figure S2: FT-IR spectra of compound **2** and (a) 3-chlorobenzoic acid and (b) the 1:1 molecular salt of 3-chlorobenzoic acid:2-amino-4-chloropyridine; Figure S3: FT-IR spectra of compound **3** and its starting materials (a) 4-chlorobenzoic acid, (b) 2-amino-4-chloropyridine, and (c) the 1:1 molecular salt of 4-chlorobenzoic acid:2-amino-4-chloropyridine). Figure S4 shows the 2D reduced density gradient (RDG) graphs and 3D noncovalent interactions (NCI plots) for the clusters of compounds, **1** halogen bonding, and **2** and **3**. Powder XRD patterns of compounds **1**, **2**, and **3** (Figures S5–S7), Figure S8a,c UV-visible spectra of compounds **1** and **2**, showing a decreasing pattern upon an increase in concentration, and Figure S8b is compound 2, showing a smaller or limited decrease in absorbance at 517 nm upon increasing the concentration. Figure S9, The 2D reduced density gradient (RDG) and 3D noncovalent interactions (NCI plots) for cluster of compounds 1 having dominant hydrogen bonding. The three types of interactions including hydrogen bonding, London dispersion interaction and repulsive interactions are represented by blue, green and red color, respectively.

Author Contributions: Conceptualization, T.A. and E.K.; methodology, T.A.; software, N.K., M.A. and T.M.; validation, M.A., T.M. and E.K.; investigation, T.A.; resources, E.K.; writing—original draft preparation, T.A., N.K., M.S. and E.K; writing—review and editing, E.K.; visualization, N.K, T.M. and E.K.; supervision, E.K.; project administration, E.K. All authors have read and agreed to the published version of the manuscript.

Funding: This research received no funding.

Institutional Review Board Statement: Not applicable.

Informed Consent Statement: Not applicable.

Data Availability Statement: All data pertaining to the instant publication is included in the main text and a Supporting Information file.

Conflicts of Interest: The authors declare that they have no known competing interest or personal relationship that could have appeared to influence the work reported in this paper.

References

1. Childs, S.L.; Stahly, G.P.; Park, A. The salt−cocrystal continuum: The influence of crystal structure on ionization state. *Mol. Pharm.* **2007**, *4*, 323–338. [CrossRef]
2. Stahly, G.P. Diversity in single-and multiple-component crystals. The search for and prevalence of polymorphs and cocrystals. *Cryst. Growth Des.* **2007**, *7*, 1007–1026. [CrossRef]
3. Stahl, P.H.; Wermuth, C.G. Handbook of pharmaceutical salts: Properties, selection and use. *Chem. Int.* **2002**, *24*, 21.
4. Brittain, H.G. Strategy for the Prediction and Selection of Drug Substance Salt Forms. *Pharm. Technol.* **2007**, *31*, 78–84.
5. Lemmerer, A.; Esterhuysen, C.; Bernstein, J. Synthesis characterization molecular modeling of a pharmaceutical co-crystal:(2-chloro-4-nitrobenzoic acid):(nicotinamide). *J. Pharm. Sci.* **2010**, *99*, 4054–4071. [CrossRef] [PubMed]
6. Santra, R.; Ghosh, N.; Biradha, K. Crystal engineering with acid and pyridine heteromeric synthon: Neutral and ionic co-crystals. *New J. Chem.* **2008**, *32*, 1673–1676. [CrossRef]
7. Bosch, E. Chain-link hydrogen-bonded capsules. *CrystEngComm* **2007**, *9*, 191–198. [CrossRef]
8. Childs, S.L.; Hardcastle, K.I. Cocrystals of piroxicam with carboxylic acids. *Cryst. Growth Des.* **2007**, *7*, 1291–1304. [CrossRef]
9. Wenger, M.; Bernstein, J. Designing a Cocrystal of γ-Amino Butyric Acid. *Angew. Chem. Int. Ed.* **2006**, *45*, 7966–7969. [CrossRef]
10. Aakeröy, C.B.; Salmon, D.J. Building co-crystals with molecular sense and supramolecular sensibility. *CrystEngComm* **2005**, *7*, 439–448. [CrossRef]
11. Metrangolo, P.; Neukirch, H.; Pilati, T.; Resnati, G. Halogen bonding based recognition processes: A world parallel to hydrogen bonding. *Acc. Chem. Res.* **2005**, *38*, 386–395. [CrossRef]
12. Metrangolo, P.; Meyer, F.; Pilati, T.; Proserpio, D.M.; Resnati, G. Highly Interpenetrated Supramolecular Networks Supported by N I Halogen Bonding. *Chem. Eur. J.* **2007**, *13*, 5765–5772. [CrossRef] [PubMed]
13. Cincic, D.; Friscic, T.; Jones, W. A stepwise mechanism for the mechanochemical synthesis of halogen-bonded cocrystal architectures. *J. Am. Chem. Soc.* **2008**, *130*, 7524–7525. [CrossRef] [PubMed]
14. Cinčić, D.; Friščić, T.; Jones, W. Isostructural Materials Achieved by Using Structurally Equivalent Donors and Acceptors in Halogen-Bonded Cocrystals. *Chem. A Eur. J.* **2008**, *14*, 747–753. [CrossRef] [PubMed]
15. Shirman, T.; Freeman, D.; Posner, Y.D.; Feldman, I.; Facchetti, A.; van der Boom, M.E. Assembly of crystalline halogen-bonded materials by physical vapor deposition. *J. Am. Chem. Soc.* **2008**, *130*, 8162–8163. [CrossRef] [PubMed]
16. Barooah, N.; Sarma, R.J.; Baruah, J.B. Solid-state hydrogen bonded assembly of N, N′-bis (glycinyl)-pyromellitic diimide with aromatic guests. *CrystEngComm* **2006**, *8*, 608–615. [CrossRef]
17. Nishio, M.; Hirota, M.; Umezawa, Y. *The CH/π Interaction: Evidence, Nature, and Consequences*; John Wiley & Sons: Hoboken, NJ, USA, 1998; Volume 21.
18. Fedorov, A.Y.; Rychkov, D. Comparison of different computational approaches for unveiling the high-pressure behavior of organic crystals at a molecular level. Case study of tolazamide polymorphs. *J. Struct. Chem.* **2020**, *61*, 1356–1366. [CrossRef]
19. Metrangolo, P.; Milani, R.; Pilati, T.; Priimagi, A.; Resnati, G.; Terraneo, G. The Halogen Bond. *Chem. Rev.* **2016**, *116*, 2478.
20. Aakeroy, C.B.; Chopade, P.D.; Desper, J. Establishing a hierarchy of halogen bonding by engineering crystals without disorder. *Cryst. Growth Des.* **2013**, *13*, 4145–4150. [CrossRef]
21. Karanam, M.; Choudhury, A.R. Study of halogen-mediated weak interactions in a series of halogen-substituted azobenzenes. *Cryst. Growth Des.* **2013**, *13*, 4803–4814. [CrossRef]
22. Metrangolo, P.; Resnati, G. Halogen versus hydrogen. *Science* **2008**, *321*, 918–919. [CrossRef]
23. Cardillo, P.; Corradi, E.; Lunghi, A.; Meille, S.V.; Messina, M.T.; Metrangolo, P.; Resnati, G. The N···I intermolecular interaction as a general protocol for the formation of perfluorocarbon–hydrocarbon supramolecular architectures. *Tetrahedron* **2000**, *56*, 5535–5550. [CrossRef]
24. Jennifer, S.J.; Muthiah, P.T. Design of co-crystals/salts of some Nitrogenous bases and some derivatives of thiophene carboxylic acids through a combination of hydrogen and halogen bonds. *Chem. Cent. J.* **2014**, *8*, 1–22. [CrossRef]

25. Prri, A.; Cabriella, G.; Metrabgolo, P.; Resbati, G. The halogen bond in the design of functional supramolecular materials: Recent advances. *Acc. Chem. Res.* **2013**, *46*, 2686–2695.
26. De Santis, A.; Forni, A.; Liantonio, R.; Metrangolo, P.; Pilati, T.; Resnati, G. N···Br Halogen Bonding: One-Dimensional Infinite Chains through the Self-Assembly of Dibromotetrafluorobenzenes with Dipyridyl Derivatives. *Chem.—A Eur. J.* **2003**, *9*, 3974–3983. [CrossRef] [PubMed]
27. Auffinger, P.; Hays, F.A.; Westhof, E.; Ho, P.S. Halogen bonds in biological molecules. *Proc. Natl. Acad. Sci. USA* **2004**, *101*, 16789–16794. [CrossRef] [PubMed]
28. Politzer, P.; Murray, J.S.; Clark, T. Halogen bonding and other σ-hole interactions: A perspective. *Phys. Chem. Chem. Phys.* **2013**, *15*, 11178–11189. [CrossRef] [PubMed]
29. Bilewicz, E.; Rybarczyk-Pirek, A.J.; Dubis, A.T.; Grabowski, S.J. Halogen bonding in crystal structure of 1-methylpyrrol-2-yl trichloromethyl ketone. *J. Mol. Struct.* **2007**, *829*, 208–211. [CrossRef]
30. Wang, H.; Wang, W.; Jin, W.J. σ-Hole bond vs π-hole bond: A comparison based on halogen bond. *Chem. Rev.* **2016**, *116*, 5072–5104. [CrossRef]
31. Clark, T.; Hennemann, M.; Murray, J.S.; Politzer, P. Halogen bonding: The σ-hole. *J. Mol. Model.* **2007**, *13*, 291–296. [CrossRef]
32. Politzer, P.; Murray, J.S.; Clark, T. σ-Hole bonding: A physical interpretation. In *Halogen Bonding I*; Springer International Publishing A.G. Switzerland: Cham, Switzerland, 2014; pp. 19–42.
33. Bui, T.T.T.; Dahaoui, S.; Lecomte, C.; Desiraju, G.R.; Espinosa, E. The Nature of Halogen···Halogen Interactions: A Model Derived from Experimental Charge-Density Analysis. *Angew. Chem.* **2009**, *121*, 3896–3899. [CrossRef]
34. Ibrahim, M.A.A.; Moussa, N.A.M. Unconventional Type III Halogen···Halogen Interactions: A Quantum Mechanical Elucidation of σ-Hole···σ-Hole and Di-σ-Hole Interactions. *ACS Omega* **2020**, *5*, 21824–21835. [CrossRef] [PubMed]
35. Baldrighi, M.; Cavallo, G.; Chierotti, M.R.; Gobetto, R.; Metrangolo, P.; Pilati, T.; Resnati, G.; Terraneo, G. Halogen bonding and pharmaceutical cocrystals: The case of a widely used preservative. *Mol. Pharm.* **2013**, *10*, 1760–1772. [CrossRef] [PubMed]
36. La Motta, C.; Sartini, S.; Mugnaini, L.; Salerno, S.; Simorini, F.; Taliani, S.; Marini, A.M.; Da Settimo, F.; Lavecchia, A.; Novellino, E. Exploiting the pyrazolo [3, 4-d] pyrimidin-4-one ring system as a useful template to obtain potent adenosine deaminase inhibitors. *J. Med. Chem.* **2009**, *52*, 1681–1692. [CrossRef] [PubMed]
37. Khan, E. Pyridine Derivatives as Biologically Active Precursors; Organics and Selected Coordination Complexes. *ChemistrySelect* **2021**, *6*, 3041–3064. [CrossRef]
38. Ullah, I.; Khan, E.; Zhang, Z.; Xiang, S.; Chen, C.; Li, L. Synthesis, crystal growth and supramolecular chemistry of 4-dimethylaminopyridinium salts of benzoates and a phenolate ion. *Z. Phys. Chem.* **2023**, *237*, 1381–1408. [CrossRef]
39. Khan, E.; Khan, A.; Gul, Z.; Ullah, F.; Tahir, M.N.; Khalid, M.; Asif, H.M.; Asim, S.; Braga, A.A.C. Molecular salts of terephthalic acids with 2-aminopyridine and 2-aminothiazole derivatives as potential antioxidant agents; Base-Acid-Base type architectures. *J. Mol. Struct.* **2020**, *1200*, 127126. [CrossRef]
40. Tolstoy, P.M.; Smirnov, S.N.; Shenderovich, I.G.; Golubev, N.S.; Denisov, G.S.; Limbach, H.-H. NMR studies of solid state—Solvent and H/D isotope effects on hydrogen bond geometries of 1: 1 complexes of collidine with carboxylic acids. *J. Mol. Struct.* **2004**, *700*, 19–27. [CrossRef]
41. Ishida, H.; Fukunaga, T. 3-Cyanopyridine–2-chloro-4-nitrobenzoic acid (1/1). *Acta Crystallogr. Sect. E Struct. Rep. Online* **2004**, *60*, o1664–o1665. [CrossRef]
42. Oruganti, M.; Nechipadappu, S.K.; Khade, P.A.; Trivedi, D.R. Solid-state versatility of the molecular salts/cocrystals of 2-chloro-4-nitrobenzoic acid: A case study on halogen bonds. *ACS Omega* **2017**, *2*, 7146–7162. [CrossRef]
43. Cruz-Cabeza, A.J. Acid–base crystalline complexes and the p K a rule. *CrystEngComm* **2012**, *14*, 6362–6365. [CrossRef]
44. Delori, A.; Galek, P.T.; Pidcock, E.; Patni, M.; Jones, W. Knowledge-based hydrogen bond prediction and the synthesis of salts and cocrystals of the anti-malarial drug pyrimethamine with various drug and GRAS molecules. *CrystEngComm* **2013**, *15*, 2916–2928. [CrossRef]
45. Morissette, S.L.; Almarsson, Ö.; Peterson, M.L.; Remenar, J.F.; Read, M.J.; Lemmo, A.V.; Ellis, S.; Cima, M.J.; Gardner, C.R. High-throughput crystallization: Polymorphs, salts, co-crystals and solvates of pharmaceutical solids. *Adv. Drug Deliv. Rev.* **2004**, *56*, 275–300. [CrossRef] [PubMed]
46. Patra, R.; Titi, H.M.; Goldberg, I. Crystal engineering of molecular networks: Tailoring hydrogen-bonding self-assembly of tin-tetrapyridylporphyrins with multidentate carboxylic acids as axial ligands. *Cryst. Growth Des.* **2013**, *13*, 1342–1349. [CrossRef]
47. Hanif, M.; Khan, E.; Khalid, M.; Tahir, M.N.; de Alcântara Morais, S.F.; Braga, A.A.C. 2-Amino-3-methylpyridinium, 2-amino-4-methylbenzothiazolium and 2-amino-5-chloropyridinium salts. Experimental and theoretical findings. *J. Mol. Struct.* **2020**, *1222*, 128914. [CrossRef]
48. Khan, E.; Khalid, M.; Gul, Z.; Shahzad, A.; Tahir, M.N.; Asif, H.M.; Asim, S.; Braga, A.A.C. Molecular structure of 1, 4-bis (substituted-carbonyl) benzene: A combined experimental and theoretical approach. *J. Mol. Struct.* **2020**, *1205*, 127633. [CrossRef]
49. Khan, S.; Zahoor, M.; Rahman, M.U.; Gul, Z. Cocrystals; basic concepts, properties and formation strategies. *Z. Für Phys. Chem.* **2023**, *237*, 273–332. [CrossRef]
50. Yamashita, H.; Hirakura, M.Y.; Yuda, T.; Teramura, K. Terada, Detection of cocrystal formation based on binary phase diagrams using thermal analysis. *Pharm. Res.* **2013**, *30*, 70–80. [CrossRef]

51. Islam, N.U.; Umar, M.N.; Khan, E.; Al-Joufi, F.A.; Abed, S.N.; Said, M.; Ullah, H.; Iftikhar, M.; Zahoor, M.; Khan, F.A. Levofloxacin Cocrystal/Salt with Phthalimide and Caffeic Acid as Promising Solid-State Approach to Improve Antimicrobial Efficiency. *Antibiotics* **2022**, *11*, 797. [CrossRef]
52. Chiarella, R.A.; Davey, R.J.; Peterson, M.L. Making co-crystals the utility of ternary phase diagrams. *Cryst. Growth Des.* **2007**, *7*, 1223–1226. [CrossRef]
53. Rychkov, D.A.; Stare, J.; Boldyreva, E.V. Pressure-driven phase transition mechanisms revealed by quantum chemistry: L-serine polymorphs. *Phys. Chem. Chem. Phys.* **2017**, *19*, 6671–6676. [CrossRef] [PubMed]
54. Rychkov, D.; Arkhipov, S.; Boldyreva, E. Structure-forming units of amino acid maleates. Case study of l-valinium hydrogen maleate. *Acta Crystallogr. Sect. B* **2016**, *72*, 160–163. [CrossRef] [PubMed]
55. Spackman, P.R.; Turner, M.J.; McKinnon, J.J.; Wolff, S.K.; Grimwood, D.J.; Jayatilaka, D.; Spackman, M.A. CrystalExplorer: A program for Hirshfeld surface analysis, visualization and quantitative analysis of molecular crystals. *J. Appl. Crystallogr.* **2021**, *54*, 1006–1011. [CrossRef] [PubMed]
56. Kosar, N.; Gul, S.; Ayub, K.; Bahader, A.; Gilani, M.A.; Arshad, M.; Mahmood, T. Significant nonlinear optical response of alkaline earth metals doped beryllium and magnesium oxide nanocages. *Mater. Chem. Phys.* **2020**, *242*, 122507. [CrossRef]
57. Hanif, M.; Kosar, N.; Mahmood, T.; Muhammad, M.; Ullah, F.; Tahir, M.N.; Ribeiro, A.I.; Khan, E. Schiff Bases Derived from 2-Amino-6-methylbenzothiazole, 2-Amino-5-chloropyridine and 4-Chlorobenzaldehyde: Structure, Computational Studies and Evaluation of Biological Activity. *Chem. Sel.* **2022**, *7*, e202203386. [CrossRef]
58. Politzer, P.; Murray, J.S. An Overview of Strengths and Directionalities of Noncovalent Interactions: σ-Holes and π-Holes. *Crystals* **2019**, *9*, 165. [CrossRef]
59. Lu, T.; Chen, F. Multiwfn: A multifunctional wavefunction analyzer. *J. Comput. Chem.* **2012**, *33*, 580–592. [CrossRef] [PubMed]
60. Tan, S.L.; Jotani, M.M.; Tiekink, E.R.T. Utilizing Hirshfeld surface calculations, non-covalent interaction (NCI) plots and the calculation of interaction energies in the analysis of molecular packing. *Acta Crystallogr. Sect. E* **2019**, *75*, 308–318. [CrossRef]
61. Molyneux, P. The use of the stable free radical diphenylpicrylhydrazyl (DPPH) for estimating antioxidant activity. Songklanakarin. *J. Sci. Technol.* **2004**, *26*, 211–219.
62. Liu, L.; Zou, D.; Zhang, Y.; Zhang, Q.; Feng, Y.; Guo, Y.; Liu, Y.; Zhang, X.; Cheng, G.; Wang, C. Pharmaceutical salts/cocrystals of enoxacin with dicarboxylic acids: Enhancing in vitro antibacterial activity of enoxacin by improving the solubility and permeability. *Eur. J. Pharm. Biopharm.* **2020**, *154*, 62–73. [CrossRef]
63. Bruker. *APEX3, SAINT and SADABS*; Crystallography Software Suite, Bruker AXS, Inc.: Madison, WI, USA, 2016.
64. Altomare, A.; Burla, M.C.; Camalli, M.; Cascarano, G.L.; Giacovazzo, C.; Guagliardi, A.; Moliterni, A.G.G.; Polidori, G.; Spagna, R. SIR97: A new tool for crystal structure determination and refinement. *J. Appl. Crystallogr.* **1999**, *32*, 115–119. [CrossRef]
65. Sheldrick, G. Crystal structure refinement with SHELXL. *Acta Crystallogr. Sect. C* **2015**, *71*, 3–8. [CrossRef] [PubMed]
66. Farrugia, L. WinGX suite for small-molecule single-crystal crystallography. *J. Appl. Crystallogr.* **1999**, *32*, 837–838. [CrossRef]
67. Spek, A. Structure validation in chemical crystallography. *Acta Crystallogr. Sect. D* **2009**, *65*, 148–155. [CrossRef]
68. Frisch, M.J.; Trucks, G.W.; Schlegel, H.B.; Scuseria, G.E.; Robb, M.A.; Cheeseman, J.R.; Scalmani, G.; Barone, V.; Petersson, G.A.; Nakatsuji, H.; et al. *Fox Gaussian 09, Revision A.02*; Gaussian, Inc.: Wallingford, CT, USA, 2016.
69. John, D. *Roy, Keith, Todd, Millam, GaussView 5.0*; Semichem Inc.: Shawnee Mission, KS, USA, 2009.
70. Tretyakova, I.S.; Rychkov, D.A.; Lomovskiy, I.O. Computational study of chemical phenol glycosylation mechanism in the gas phase for modeling direct glycoconjugate formation in raw plant material. *Comput. Theor. Chem.* **2023**, *1225*, 114182. [CrossRef]
71. Bursch, M.; Mewes, J.M.; Hansen, A.; Grimme, S. Best-Practice DFT Protocols for Basic Molecular Computational Chemistry. *Angew. Chem. Int. Ed.* **2022**, *61*, e202205735. [CrossRef]
72. Hirshfeld, F.L. Bonded-atom fragments for describing molecular charge densities. *Theor. Chim. Acta* **1977**, *44*, 129–138. [CrossRef]
73. Balouiri, M.; Sadiki, M.; Ibnsouda, S.K. Methods for in vitro evaluating antimicrobial activity: A review. *J. Pharm. Anal.* **2016**, *6*, 71–79. [CrossRef]
74. Asghar, A.; Tan, Y.C.; Zahoor, M.; Zainal Abidin, S.A.; Yow, Y.Y.; Khan, E.; Lahiri, C. A scaffolded approach to unearth potential antibacterial components from epicarp of Malaysian *Nephelium lappaceum* L. *Sci. Rep.* **2021**, *11*, 13859. [CrossRef]
75. Baliyan, S.; Mukherjee, R.; Priyadarshini, A.; Vibhuti, A.; Gupta, A.; Pandey, R.P.; Chang, C.M. Determination of Antioxidants by DPPH Radical Scavenging Activity and Quantitative Phytochemical Analysis of Ficus religiosa. *Molecules* **2022**, *27*, 1326. [CrossRef]